# Assessing safety of nature-based flood defenses: Dealing with extremes and uncertainties

Vincent Vuik [a,b,*], Saskia van Vuren [a,c], Bas W. Borsje [d,e], Bregje K. van Wesenbeeck [a,f], Sebastiaan N. Jonkman [a]

[a] Delft University of Technology, Faculty of Civil Engineering and Geosciences, P.O. Box 5048, 2600 GA, Delft, the Netherlands
[b] HKV Consultants, P.O. Box 2120, 8203 AC, Lelystad, the Netherlands
[c] Rijkswaterstaat, P.O. Box 2232, 3500 GE, Utrecht, the Netherlands
[d] University of Twente, Water Engineering & Management, P.O. Box 217, 7500 AE, Enschede, the Netherlands
[e] Board Young Waddenacademie, Ruiterskwartier 121a, 8911 BS, Leeuwarden, the Netherlands
[f] Deltares, P.O. Box 177, 2600 MH, Delft, the Netherlands

A B S T R A C T

Vegetated foreshores adjacent to engineered structures (so-called hybrid flood defenses), are considered to have high potential in reducing flood risk, even in the face of sea level rise and increasing storminess. However, foreshores such as salt marshes and mangrove forests are generally characterized by relatively strong temporal and spatial variations in geometry and vegetation characteristics (e.g., stem height and density), which causes uncertainties with regards to their protective value under extreme storm conditions. Currently, no method is available to assess the failure probability of a hybrid flood defense, taking into account the aforementioned uncertainties. This paper presents a method to determine the failure probability of a hybrid flood defense, integrating models and stochastic parameters that describe dike failure and wave propagation over a vegetated foreshore. Two dike failure mechanisms are considered: failure due to (i) wave overtopping and (ii) wave impact on revetments. Results show that vegetated foreshores cause a reduction in failure probability for both mechanisms. This effect is more pronounced for wave impact on revetments than for wave overtopping, since revetment failure occurs at relatively low water levels. The relevance of different uncertainties depends on the protection level and associated dike height and strength. For relatively low dikes (i.e., low protection levels), vegetation remains stable in design conditions, and plays an important role in reducing wave loads. In case of higher protection levels, hence for more robust dikes, vegetation is less important than foreshore geometry, because of expected stem breakage of the vegetation under these more extreme conditions. The integrated analysis of uncertainties in hydraulic loads, dike geometry and foreshore characteristics in this paper enables the comparison between nature-based flood defenses and traditionally engineered solutions, and allows coastal engineers to design hybrid flood defenses worldwide.

## 1. Introduction

Climate change, land subsidence and population growth in coastal areas lead to an increase in flood hazards and in its consequent economic damage and loss of life (Mendelsohn et al., 2011). Frequency and destructiveness of floods will steadily increase if sustainable flood risk reducing measures are not adequately implemented. Flood risk can be reduced by various interventions, ranging from construction and maintenance of dikes and dams to mitigation measures such as flood warning systems (Carsell et al., 2004) and evacuation strategies (Kolen and Helsloot, 2014). In a systems approach, multiple lines of defense are perpetuated, integrating structural and non-structural flood protection with coastal restoration (Lopez, 2009). Within this context, efforts are being made to make greater use of nature-based approaches to flood risk reduction (Spalding et al., 2014; Bridges et al., 2015). Coastal ecosystems, such as salt marshes, mangrove forests and reefs, can contribute to flood risk reduction by surge attenuation (Wamsley et al., 2010), wave energy dissipation and erosion reduction (Gedan et al., 2011). On the long term, they can raise their bottom surface because of their sediment trapping capacity, thereby counterbalancing the effect of sea level rise

---

(Mckee et al., 2007). However, these ecosystems are under threat worldwide because of sediment starvation (Adam, 2002; Willemsen et al., 2016), land reclamation (Zhao et al., 2004), deforestation (Bradshaw et al., 2007) and eutrophication (Deegan et al., 2012). This has resulted in a global loss rate of 1–3% of total area per year (Duarte et al., 2013). This trend necessitates conservation, sustainable management and restoration of coastal ecosystems to preserve, or even enhance their role in flood risk reduction. Coastal ecosystems can work stand-alone, but can also be incorporated into hybrid solutions, where ecosystems are utilized as vegetated foreshores along engineered structures. Depth-induced wave breaking, bottom friction and wave attenuation by vegetation lead to a reduction in wave energy over the foreshore, which reduces the required strength and dimensions of structural interventions (Vuik et al., 2016). Hybrid solutions are especially suited for low-lying and flat delta areas, since ecosystems can efficiently reduce wave energy, but are not able to keep out the surge completely.

Although vegetated foreshores are present along many coastlines, their role for coastal protection is rarely incorporated into flood protection strategies, and most examples of successful implementation concern small-scale pilot projects (Spalding et al., 2014). One of the causes is a lack of methods for testing hybrid solutions according to engineering standards for safety, often expressed by means of the probability of failure (Van Wesenbeeck et al., 2014). With state-of-the-art statistical and probabilistic techniques, it is possible to determine a failure probability and an optimal design of a traditional dike, considering the stochastic behavior of both load and strength (e.g. Vrijling (2001); Voortman (2003); Steenbergen et al. (2004)), with applications in for example the Netherlands (Jonkman et al., 2008), the UK (Buijs et al., 2004) and China (Zhang and Xu, 2011). Some studies have applied probabilistic methods to sandy shorelines, to describe coastal cliff recession (Hall et al., 2002) and dune erosion (Den Heijer et al., 2012; Vuik et al., 2017). Uncertainties are even more relevant for more complex flood defense systems like hybrid solutions, which combine ecological and engineering features. However, no methods are available to assess the failure probability of hybrid systems and to incorporate effects of relevant uncertainties, such as spatial and temporal variations in vegetation characteristics, wave attenuation by flexible vegetation, and stability of vegetation under extreme wave forcing. Consequently, it is difficult to assess effects of vegetated foreshores on safety.

The aim of this paper is to assess the failure probability of nature-based flood defenses, more specifically, for a configuration with a dike accompanied by a vegetated foreshore. A probabilistic model framework is developed, in which uncertainties in hydraulic loads, characteristics and functioning of the vegetated foreshore, and strength of the dike are taken into account. The two most prevalent wave-driven failure mechanisms are considered: (i) erosion of the crest and inner slope of the dike due to wave overtopping, and (ii) erosion of the revetment or grass cover on the outer slope due to impact of breaking waves. Different foreshore configurations are defined, inspired by dikes and salt marshes bordering the Dutch Wadden Sea. This paper shows how these foreshore configurations affect the failure probability of the flood defense, and to what extent different variables and processes influence this failure probability.

## 2. Methods

### 2.1. System description

In hybrid solutions, ecosystems are utilized as vegetated foreshores along engineered structures. The combined dike-foreshore system is schematized, as shown in Fig. 1. Parameters will be introduced throughout the methods section, and are summarized in Appendix A. The combined characteristics of the dike, foreshore and vegetation determine the strength of the system. Hydrodynamic boundary conditions depend on the wind speed $U_{10}$ (m/s) and are represented by a still water level $\zeta$ (m MSL), significant wave height $H_{m0}$ (m) and a characteristics wave period, such as the peak period $T_p$ (s) or the spectral mean wave period
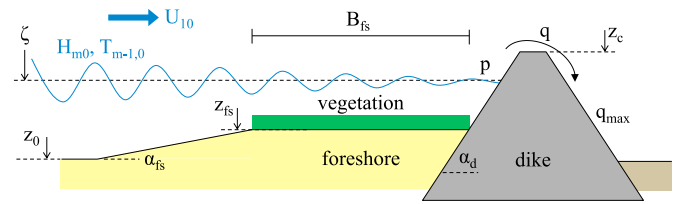


**Fig. 1.** Schematic representation of a dike-foreshore system, with a stretched vertical scale. System characteristics and computed quantities are shown in black, boundary conditions in blue, and model parameters in red. Parameters will be introduced throughout the methods section, and are summarized in Appendix A. (For interpretation of the references to color in this figure legend, the reader is referred to the Web version of this article.)

$T_{m-1,0}$ (s). The foreshore is characterized by a flat part of $B_{fs}$ meter wide and an elevation $z_{fs}$ (m MSL), which is naturally close to high water spring, because of sediment deposition by the tide (Allen, 2000; Borsje et al., 2017). Offshore from the marsh edge, the profile slopes under an angle $\alpha_{fs}$ to the bed level $z_0$ (m MSL) of the tidal flats. The marsh vegetation is described by a set of physical characteristics and model parameters, which together determine the wave attenuating capacity and stability against stem breakage. This will be discussed in section 2.2.

Two different failure mechanisms of the dike are considered. Firstly, failure due to wave overtopping over the dike with crest level $z_c$ (m MSL) and slope angle $\alpha_d$, which occurs when the wave overtopping discharge $q$ (l/s per m width) exceeds a maximum tolerable value $q_{max}$ that depends on the erosion resistance of the crest and inner slope of the dike (section 2.3). Secondly, failure due to wave impacts $p$ (N/m$^2$) on the outer slope, which leads to damage of the cover and subsequent erosion of the underlying dike core material if the storm duration exceeds a threshold value. For this second failure mechanism, covers with grass (section 2.4) and asphalt (section 2.5) are considered.

A model framework (Fig. 2) is applied to compute the failure probability of a dike, including the effect of a vegetated foreshore. Local water levels and wave characteristics are generated by wind and tide. Wind speed, water level and offshore wave conditions are applied as boundary conditions. Without foreshore, a flat bottom at $z_0$ is considered. Presence of the vegetated foreshore affects the wave conditions, impact, run-up and, in extreme cases, overtopping over the dike. The framework consists of modules to account for foreshore effects (section 2.2), wave overtopping (section 2.3) or wave impact (sections 2.4 and 2.5).
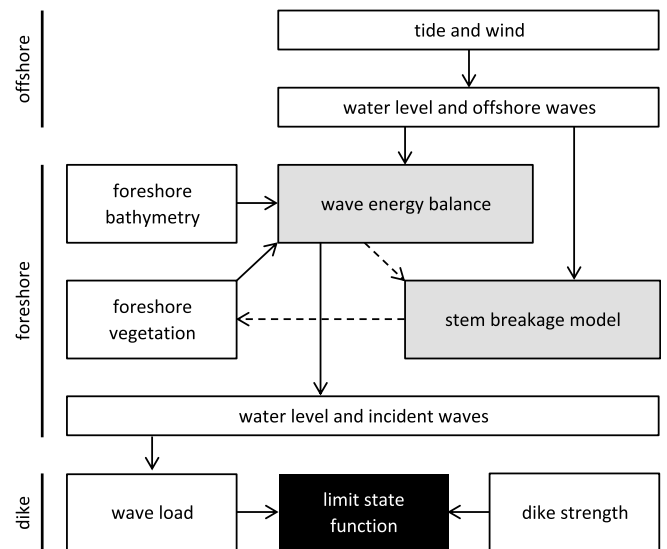


**Fig. 2.** Model framework to compute a probability of failure. A limit state function $Z$ is defined, and given by the difference between strength and load. The definitions of dike strength and wave load differ per failure mechanism.

A limit state function (LSF) describes dike failure in terms of the difference between strength ($R$) and load ($S$): $Z = R - S$. Both load and strength are considered as stochastic (i.e., uncertain) variables. Failure occurs when $Z < 0$. The corresponding probability that the dike fails is $P(Z < 0)$, shortly denoted as the probability of failure $P_f$. The framework is applied to compute this probability.

## 2.2. Modeling of foreshore effects

The foreshore is included in the framework of Fig. 2 via a one-dimensional wave energy balance:

$$\frac{dEc_g}{dx} = S_{in} - S_{ds,w} - S_{ds,b} - S_{ds,f} - S_{ds,v}, \tag{1}$$

where $E = (1/8)\rho g H_{rms}^2$ is wave energy density (J/m$^2$), $H_{rms}$ root mean square wave height (m), $\rho$ density of water (kg/m$^3$), $g$ gravitational acceleration (m/s$^2$), $c_g$ group velocity (m/s), and $x$ distance (m) along the foreshore. The right hand side of Eq. (1) consists of different source terms (J m$^{-2}$ s$^{-1}$): energy input by wind ($S_{in}$), and energy dissipation due to whitecapping ($S_{ds,w}$), depth-induced wave breaking ($S_{ds,b}$), bottom friction ($S_{ds,f}$) and vegetation ($S_{ds,v}$). The energy balance is discretized, using a simple first order numerical scheme with step size $\Delta x = 5$ m. The offshore wave period $T_p$ is considered in the energy balance. In addition, the equation of Hofland et al. (2017) is used to account for a possible increase in spectral mean wave period $T_{m-1,0}$ over the shallow foreshore, based on the difference in depth between offshore mudflats ($z_0$) and foreshore ($z_{fs}$). Dissipation due to wave breaking, bottom friction and vegetation will be dominant on vegetated foreshores. Vegetation is described by cylinders with stem height $h_v$ (m), stem diameter $b_v$ (m), stem density $N_v$ (stems/m$^2$) and bulk drag coefficient $\tilde{C}_D$ (−). The dissipation formula of Mendez and Losada (2004) is implemented to account for wave attenuation by this vegetation. For depth-induced wave breaking, the formula of Battjes and Janssen (1978) is used, in which the breaker parameter $\gamma$ (−) follows from Battjes and Stive (1985). Bottom friction is represented by a roughness height $k_N$ (m), following Madsen et al. (1988). The energy balance is primarily meant for computations over short distances, less than 1 or 2 km. For longer distances, a one-dimensional approach is mostly insufficient. However, to avoid an overestimation of the wave height reduction for relatively long foreshores, the processes wind input (due to Snyder et al. (1981)) and whitecapping (due to Komen et al. (1984)) are added. All these model descriptions correspond with the implementations in the spectral wave model SWAN (Booij et al., 1999). If the wave-induced bending stresses exceed the plant's flexural strength, the stem will fold or break near the bottom (Rupprecht et al., 2017). The stem breakage model developed in Vuik et al. (2018) is implemented in the model framework of Fig. 2. This model compares the wave-induced bending stress with the flexural strength of the stems. Stem breakage occurs when the actual wave orbital velocity exceeds the stem's critical velocity, for stems with a circular cross-section expressed as

$$u_{crit} = \sqrt{\frac{\sigma_{max}\pi\left(b_v^4 - b_{v,in}^4\right)}{8A_c\rho b_v^2\left[C_D h_{v,r}^2 + 2\pi C_f(h_v - h_{v,r})h_{v,r}\right]}}, \tag{2}$$

in which $A_c$ is an empirical correction factor for the wave-induced stress (−), $h_{v,r} = (1 - f_r)h_v$ the reduced height (m) of the canopy after leaning and bending, $b_{v,in}$ the inner stem diameter in case of hollow stems (m), $C_D$ the drag coefficient for forces on cylinders (−), and $C_f$ the skin friction coefficient (−). This formula combines drag force over the reduced vegetation height and friction force over the part of the stem that leans horizontally in the flow (Luhar and Nepf, 2011). Stems are assumed to break if the amplitude of the in-canopy orbital velocity caused by the highest 10% of the waves ($H_{1/10} = 1.27 H_{m0}$) exceeds the value of the

critical velocity. Based on the variation of $u_{crit}$ over the stems due to variations in stem height, strength and diameter, a fraction of broken stems is computed. The total wave attenuation consists of a contribution by standing stems (with the original height $h_v$) and a contribution by broken stems (with a height of broken stems $h_{v,br}$). Details of this approach are described in Vuik et al. (2018).

## 2.3. Failure due to wave overtopping

The limit state function $Z$ (LSF) for wave overtopping is defined as the difference between tolerable and actual overtopping discharge:

$$Z_{ov} = q_{max} - q, \tag{3}$$

in which $q$ is the wave overtopping discharge (l/s/m), according to EurOtop (2016), and $q_{max}$ is the tolerable overtopping discharge, which depends on the erosion resistance of the dike crest and rear slope. The lower part of Fig. 2 is more specifically represented by the content of Fig. 3, in order to compute a probability of failure due to wave overtopping.

A shallow foreshore can affect the amount of overtopping by a change in wave height, wave period, and thereby wave steepness $s_0$ and Iribarren number $\zeta_{m-1,0} = tan(\alpha_d)/\sqrt{s_0}$, in which $\alpha_d$ is the dike slope angle. Three situations are distinguished in EurOtop (2016), based on $\zeta_{m-1,0}$:

1. Wind sea conditions and moderate to steep dike slopes ($\zeta_{m-1,0} < 2 - 3$), where waves will break on the dike slope;
2. A situation where a foreshore reduces wave steepness ($2 - 3 < \zeta_{m-1,0} < 5$), so that most waves will surge on the dike slope, without significant breaking;
3. A situation where heavy wave breaking on a very shallow foreshore leads to a flat wave energy spectrum without a clear peak, and where non-linear wave interactions transfer energy to infra-gravity wave frequencies ($\zeta_{m-1,0} > 7$).

The tolerable overtopping discharge $q_{max}$ represents the erosion resistance of the grass cover on the crest and rear slope of the dike. Van der Meer et al. (2009) describe in-situ overtopping tests on dikes with grass covers on clay, and the damage to the slope for different overtopping discharges. For actual dike failure, large-scale damage and erosion is relevant.

## 2.4. Failure due to wave impact on grass covers

Where the cover of the crest and rear slope is affected by overtopping waves, the outer slope is primarily loaded by the impact of breaking waves. The limit state function $Z_{gr}$ (LSF) for failure of a grass cover due to wave impact is defined as the difference (hrs) between the time required to erode the top layer with grass roots $t_{top}$ and the clay layer $t_{sub}$, and the effective duration $t_{load,eff}$ of the wave loads at a certain location on the
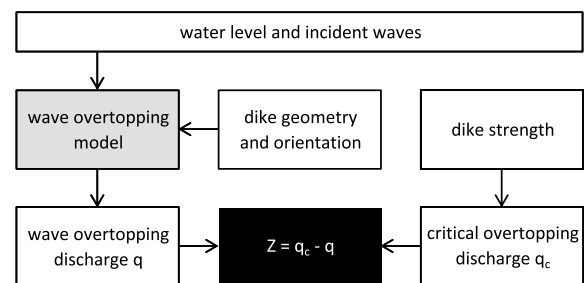


**Fig. 3.** Limit state function $Z_{gr}$ for failure of a dike due to erosion of the crest and rear slope, caused by wave overtopping. The limit state is defined, as the difference between strength (tolerable overtopping discharge) and load (actual wave overtopping discharge).

slope:

$$Z_{gr} = t_{top} + t_{sub} - t_{load,eff}. \tag{4}$$

The lower part of Fig. 2 is more specifically represented by the content of Fig. 4, in order to compute a probability of failure due to wave impact on grass covers.

Equations for the time required to erode the grass and clay layer ($t_{top} + t_{sub}$) are based on De Waal and Van Hoven (2015). The effective load duration $t_{load,eff}$ is the time span over which waves impact the dike slope at a certain location. This time span depends on (1) the time variation of the still water level and (2) the maximum distance to still water level for which waves are able to damage a grass cover. Appendix B gives a more detailed description of the formulas for failure due to wave impact on grass covers.

## 2.5. Failure due to wave impact on asphalt revetments

Failure of an asphalt revetment is a matter of fatigue. Breaking waves cause wave impacts on the dike, which leads to bending stresses in the asphalt layer. Theoretically, a crack can form when the bending stress due to an individual wave exceeds the flexural strength of the asphalt. In practice, it is more likely that asphalt will fail due to many repetitive load cycles. The model described in De Looff et al. (2006) is used to compute failure of asphalt revetments, which is based on the principle that the asphalt layer will fail when the actual number of waves exceeds the critical number of waves (Fig. 5).

The maximum number of tolerable load cycles $N_{max}$ depends on the difference between the wave-induced bending stress $\sigma$ (MPa) in the asphalt layer and the flexural strength $\sigma_{br}$ (MPa), and reads

$$\log_{10} N_{max} = V_\beta (\log_{10}(\sigma_{br}) - \log_{10}(\sigma))^{V_\alpha}, \tag{5}$$

in which $V_\alpha$ and $V_\beta$ are dimensionless parameters that describe the fatigue curve, based on laboratory tests of asphalt. Failure of the revetment occurs if the so-called Miner sum exceeds 1. A contribution to the Miner sum of $1/N_{max,i}$ is computed for all waves $i = 1..N_w$ within the load duration, where $N_{max,i}$ follows from Eq. (5).

$$Z_{as} = 1 - \sum_{i=1}^{N_w} 1/N_{max,i}. \tag{6}$$

This equation is included in logarithmic form in the model framework, to improve the convergence of the probabilistic computations:

$$Z_{as} = -\log_{10}\left(\sum_{i=1}^{N_w} 1/N_{max,i}\right). \tag{7}$$

The procedure to compute $N_w$ bending stresses $\sigma$ is included in Appendix C.
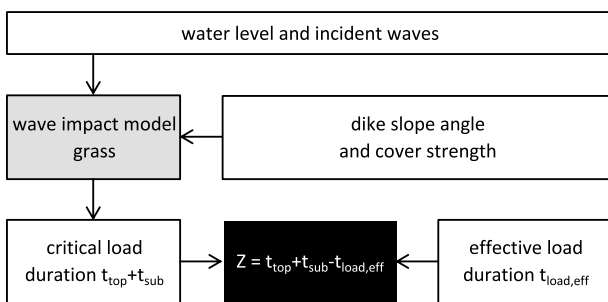
**Fig. 4.** Limit state function $Z_{gr}$ for failure of a dike due to wave impact on a grass cover on the outer slope. The limit state is defined, as the difference between strength (time required to erode the grass and clay layer, $t_c = t_{top} + t_{sub}$) and load (effective duration of wave loads on a certain point on the dike, $t_{load,eff}$).
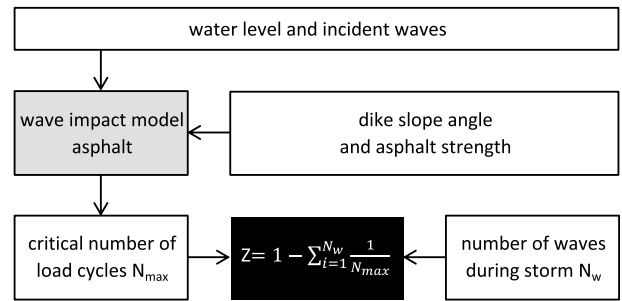
**Fig. 5.** Limit state function $Z_{as}$ for failure of a dike due to wave impact on an asphalt revetment on the outer slope. For each wave, it is determined how many of such waves the asphalt can withstand ($N_{max}$). The limit state function becomes negative (i.e., failure occurs) if the sum of $1/N_{max,i}$ over all waves ($i = 1..N_w$) exceeds 1.

## 2.6. Probabilistic method

The framework (Fig. 2) is used to compute the outcome of the LSF, Eq. (3) and (4) or (6), for any possible combination of input variables. Values of input variables are selected from their probability density functions, see Appendix A. The probabilistic method FORM (First Order Reliability Method, see Hasofer and Lind (1974)) is applied to compute a probability of failure $P_f$, using the open source implementation in OpenEarthTools (Van Koningsveld et al., 2010). In case of wave overtopping, this is the probability that the tolerable overtopping discharge is exceeded, i.e. $P_f = P(Z_{ov} < 0) = P(q > q_{max})$. FORM simplifies the mathematical problem by linearizing the LSF and transforming all probability distributions to equivalent normal distributions with mean value $\mu_i^N$ and standard deviation $\sigma_i^N$. The probability of failure $P_f$ is expressed in terms of a reliability index $\beta$ via the cumulative standard normal distribution $\Phi$:

$$P_f = \Phi(-\beta), \tag{8}$$

FORM starts in a user-defined position in the probability density functions of all variables ($i = 1..n$), for example with a relatively high value for the boundary conditions, in combination with the mean value of all other parameters. This point is the first guess of the so-called design point $X^*$. The final design point should represent the most likely parameter values associated with failure. FORM uses an iterative method to update the design point until convergence of the design point and corresponding reliability index is reached. Statistical dependence between different variables is taken into account via Gaussian correlation, characterized by Pearson's correlation coefficients. This choice is discussed in more detail in section 3.2. Correlated input variables are transformed into independent standard normal variables via Rosenblatt transformation (Rosenblatt, 1952). See Jongejan et al. (2011) for an example of application of FORM in the context of flood risk.

In each iteration, FORM tests how strong the LSF responds to a perturbation of each individual variable $X_i$. The response is expressed in terms of the partial derivative $\partial Z/\partial X_i$. Based on these partial derivatives, importance factors $\alpha_i$ are calculated (where $\sum \alpha_i = 1$). For example, a large importance factor for the marsh width $B_{fs}$ indicates a strong response of the limit state function to the standard deviation $\sigma_i^N$ of this variable. The uncertainty in foreshore width has a strong influence on the failure probability in that case.

The design point and the partial derivatives are used to compute the reliability index of the system. The reliability index increases if the design point contains parameter values far from their mean values $\mu_i^N$. A high reliability index (i.e., low $P_f$) is for example found if a dike only fails in case of extreme surge and waves, combined with a tolerable overtopping discharge far below the mean value. Based on the reliability index and the importance factors, the design point $X^*$ is expressed as

$$X_i^* = \mu_i^N - \alpha_i \beta \sigma_i^N. \tag{9}$$

Based on the sign of $\alpha_i$, load and strength variables can be distinguished. Negative importance factors correspond with load variables, such as the wind speed or the breaker parameter. Higher values of these variables lead to higher wave loads on the dike, and a higher probability of failure. A positive importance factor indicates that a variable acts as a strength parameter, for which a higher value leads to a lower probability of failure. Examples are foreshore elevation and dike crest level. Their values in the design point are below the mean value $\mu_i^N$.

The boundary conditions will usually dominate the probability of failure ($\alpha \approx -0.95$). The dike will obviously not fail without an extreme storm, whatever the foreshore characteristics or tolerable overtopping discharge will be. Therefore it is more interesting to investigate the relative influence of the other variables, disregarding the importance factors of the boundary conditions. For this means, a new quantity is defined: the relative contribution $c_i$ of each system variable. System variables ($i = 1..n_{sys}$) are variables that describe the state and functioning of the dike-foreshore system, i.e., all variables in Appendix A, except the boundary conditions. The relative contribution is given by

$$c_i = \frac{\alpha_i^2}{\sum\limits_{n_{sys}} \alpha_i^2}. \tag{10}$$

### 2.7. Classification of uncertainties

Different types of uncertainty can be discerned. The nature of a source of uncertainty has implications for the possibilities of reducing this uncertainty. Van Gelder (2000) distinguishes between inherent (or natural) uncertainties, statistical uncertainties and model uncertainties. Statistical uncertainties and model uncertainties are often put together, and identified as knowledge uncertainties, related to incomplete knowledge about the process under investigation (Merz and Thieken, 2005).

Inherent (or natural) uncertainty is related to the inherent variability of nature, and can be subdivided into inherent uncertainty in time and space. Inherent uncertainty in time and space is caused by temporal and spatial variations in nature, which are inherently unpredictable. Examples are the maximum water level in the next 50 year, variations in properties of individual plants, asphalt aging, marsh edge erosion and seasonal variation in vegetation characteristics (Table 1). Inherent uncertainty cannot be reduced.

Secondly, knowledge uncertainty is of interest, which can be subdivided into statistical uncertainty and model uncertainty. Statistical uncertainty has to do with the finite length of measurement time series, which causes uncertainty in the choice of a certain probability distribution type and its parameters. Time series are usually too short to ensure reliable estimates of events with a low probability of exceedance, such as the wave height with an annual exceedance probability of 1/1000. Long-term measurement campaigns can help to reduce statistical uncertainty. Also a lack of information on spatial variations can lead to statistical uncertainty. Field measurements with high spatial extent and resolution can help in reducing this source of uncertainty.

**Table 1**
Examples of inherent uncertainties, statistical uncertainties and knowledge uncertainties in hybrid flood defenses, subdivided based on their location.

| Location | Inherent uncertainty | Statistical uncertainty | Knowledge uncertainty |
|---|---|---|---|
| Offshore | Future water levels | Wave height distribution | Distribution type wave height |
| Dike | Asphalt aging | Variations in dike height | Wave overtopping model |
| Foreshore | Marsh edge erosion | Spatial variations bathymetry | Wave breaking model |
| Vegetation | Seasonality | Variations in vegetation stability | Stem breakage model |

Model uncertainty describes the imperfections of model concepts. Model concepts, concerning hybrid flood defenses, describe for example the processes of wave breaking, wave attenuation by vegetation, stem breakage due to wave action and wave overtopping over the dike (Table 1). These models can be imperfect because the physics are not fully understood, or model concepts are simplified to restrict computation time. Knowledge uncertainties can be reduced by developing more sophisticated models or probability distributions.

Uncertainties can, besides on basis of their nature, be subdivided based on their location (Walker et al., 2003). This is relevant in the context of vegetated foreshores, as there is a clear distinction between uncertainties related to the boundary conditions (wind, water level, wave conditions), the foreshore and the dike. Variables (see Appendix A) are categorized, based on their nature (inherent, statistical, and model uncertainty) and location (boundary conditions, foreshore, vegetation, dike).

## 3. Application

### 3.1. Site description

The schematized system is based on a dike with foreshore in the Wadden Sea (Fig. 6). Many kilometers of the Wadden Sea dikes of Denmark, Germany and The Netherlands are bordered by salt marshes, see Fig. 7. An extensive system of brushwood dams and drainage ditches facilitates sediment trapping, soil consolidation and vegetation growth. The system was originally meant for land reclamation. Nowadays, it is maintained to preserve the natural and agricultural values of the salt marshes (Bakker et al., 2002; Reise et al., 2010; van Loon-Steensma, 2015). During storm surges, the wave loads on the dikes are reduced due to wave breaking, bottom friction, and wave attenuation by standing vegetation. The salt marshes are elevated around mean high water, due to sediment accretion, and are between a few hundred meters and 2 km wide.

Plant species composition on these marshes progresses from a seaward zone of pioneer plants (forbs, grasses and low shrubs), such as *Salicornia europaea* (common glasswort), *Puccinellia maritima* (common saltmarsh-grass) and *Spartina anglica* (common cordgrass), to more mature, taller plant species landwards, such as *Elymus athericus* (couch grass), *Aster tripolium* (sea aster) and *Suaeda maritima* (seepweed).

The dikes are at some locations fully covered with grass, while revetments are present at other places. These revetments are generally composed of different layers, with concrete elements in the tidal zone, an asphalt layer in the wave impact zone, and a grass cover in the wave run-up zone (Fig. 8). The crest and inner slope of the dike are normally covered with grass. The crest of the Dutch Wadden Sea dikes is situated at 8–9 m MSL. Outer slope angles vary between 1:3 and 1:8. A revetment is especially required at exposed locations and on steep slopes (1:3 or 1:4). Grass is only applied in the wave impact zone on gentle slopes (at least 1:6).

### 3.2. Specification of parameters and probability distributions

Appendix A gives an overview of the variables, present in the model, including the nature and location of the uncertainty, the probability distribution type used in the simulations, and the parameters of this distribution. This section gives background information on the choice of input variables. Values are presented as mean value $\pm$ standard deviation.

#### 3.2.1. Dike geometry

The efficiency of vegetated foreshores in reducing failure probabilities is investigated for dike heights of 4, 6 and 8 m MSL, in combination with a 1:4 dike slope angle (Fig. 8). In this study, lower dike heights are considered as a proxy for areas with a lower level of protection than in the Netherlands. A standard deviation of 0.1 m in crest level and 5% in
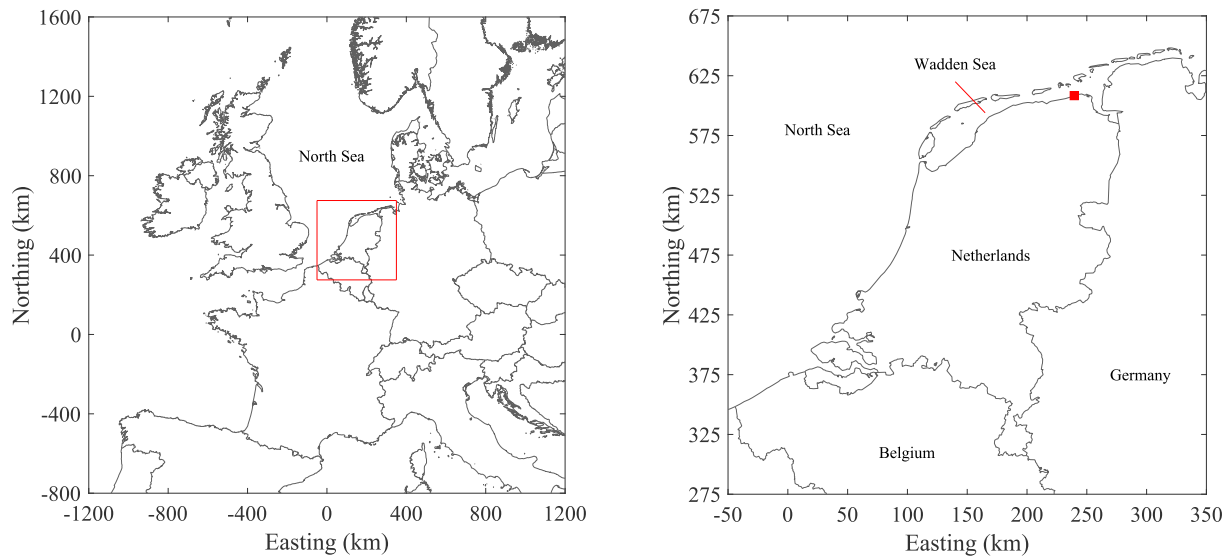
**Fig. 6.** Location of the Wadden Sea in Europe (left) and location of the salt marshes along a dike in the Netherlands (right panel, red square). (For interpretation of the references to color in this figure legend, the reader is referred to the Web version of this article.)



**Fig. 7.** Salt marshes along a Wadden Sea dike in the Netherlands (Fig. 6), with the Wadden Sea and the marshes on the right hand side of the dike. Photo: Beeldbank Rijkswaterstaat.

slope angle is considered, to account for spatial variations in dike geometry and measurement inaccuracies, corresponding with Jongejan et al. (2011). Effects of a berm, slope roughness and wave obliqueness are not considered here, for simplicity. The same 1:4 slope angle is considered to compute dike failure due to wave impact on asphalt revetments in the wave impact zone, between 2 and 6 m MSL. For dikes with a grass cover, more gentle slopes are mostly applied on coastal dikes. Therefore, a slope angle of 1:8 is used for computations on grass covers.

### 3.2.2. Wave overtopping

The distribution of tolerable overtopping discharge is based on the mean value (63 l/s/m) and standard deviation (19 l/s/m) of the values

presented in Van der Meer et al. (2009) for slopes, uniformly covered with grass on clay. Probability distributions for parameters in the formulas for the actual overtopping discharge are adopted from EurOtop (2016): $a_1$ (0.023 ± 0.003) and $b_1$ (2.70 ± 0.20) in the equation for breaking waves, $a_2$ (0.09 ± 0.0135) and $b_2$ (1.50 ± 0.15) for non-breaking waves, and $a_3$ (−0.79 ± 0.29) for very shallow foreshores (see section 2.3).

### 3.2.3. Grass covers

Grass covers can have different qualities: patchy grass on sand, open sods or homogeneous, closed sods. Only a strong grass cover on a mild slope is feasible at Wadden Sea dikes. Therefore, only a cover with closed sods on a 1:8 slope (indicated by G1) is considered here. For a description of grass quality (see Appendix B), a log-normal distribution for $C_a$ is used (1.82 ± 0.62 m). For $C_b$ and $C_c$, deterministic values are applied (−0.035/hr and 0.25 m, respectively). These values are based on laboratory experiments, and adopted from Klerk and Jongejan (2016). The effect of the small slope angle of 1:8 is taken into account via the multiplication factor $r_a$ in Eq. (13) in Appendix B. The sand fraction $f_{sand} = 0.35$, which does not influence the value of $C_d$ in Eq. (12). The total layer thickness $d_{tot}$ (grass and clay) is 0.50 ± 0.10 m.

### 3.2.4. Asphalt revetments

A new and correctly constructed asphalt revetment on a stable sandy subsoil can hardly be damaged by wave action. However, construction imperfections and asphalt aging may induce vulnerability to wave impact. Therefore, we consider the following two asphalt qualities (A1-A2): (A1) relatively low strength asphalt ($\sigma_{br} = 3.0 \pm 0.9$ MPa and $c_{sub} = 60 \pm 12$ N/m³), and (A2) asphalt of poor quality, at the end of its lifetime ($\sigma_{br} = 1.5 \pm 0.45$ MPa and $c_{sub} = 30 \pm 6$ N/m³). The asphalt thickness $d_a = 0.25 \pm 0.025$ m in both cases, and the stiffness modulus $S_a = 8000 \pm 2400$ N/m². All these parameters (see Appendix C) are based on fatigue testing of asphalt taken from 5 dikes (Kanning and Den Hengst,
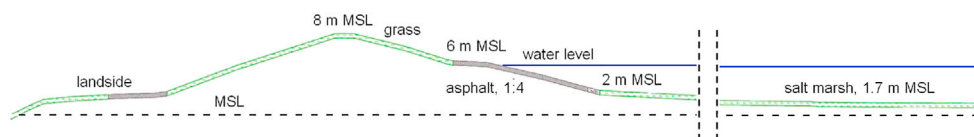


**Fig. 8.** Dike profile, based on the geometry of a dike along the Wadden Sea, with a crest level at 8 m MSL, a 1:4 sloping asphalt revetment in the wave impact zone between 2 and 6 m MSL, and a salt marsh foreshore at 1.7 m MSL.

2013). Log-normal distributions are chosen, since this distribution type fits the data well and cannot have negative values (Kanning and Den Hengst, 2013). The (deterministic) parameters that describe the fatigue curve, $V_\alpha$ and $V_\beta$, are 0.5 and 4.8, respectively.

### 3.2.5. Foreshore characteristics

The foreshore bathymetry is schematized as a vegetated flat part and a 1:100 slope from the marsh edge to the adjacent tidal flats at 0 m MSL. The foreshore elevation is set to 1.7 m MSL (Fig. 8), close to mean high water spring (MHWS). Variations in bathymetry are not computed by means of a morphological model, but via a standard deviation on foreshore width and elevation. A standard deviation of 0.2 m is applied to the foreshore elevation, representing spatial and temporal variations in topographic data of the Dutch Wadden Sea. Storm impact on the bottom surface of salt marshes is very limited, according to post-storm observation (Spencer et al., 2015) as well as large-scale wave flume experiments (Spencer et al., 2016). However, lateral erosion may cause marsh edge retreat during storms (Francalanci et al., 2013). The magnitude of this lateral erosion is hard to predict. An arbitrary standard deviation of 50 m is taken into account to assess the sensitivity of the system's probability of failure to changes in foreshore width in the time scale of a single storm.

### 3.2.6. Foreshore models

Depth-induced wave breaking depends on the breaker parameter $\gamma$ in the model, which is a function of the offshore wave steepness following Battjes and Stive (1985). A standard deviation of 0.05 is applied, estimated from Fig. 1 in Battjes and Stive (1985). Bottom friction is specified by means of a Nikuradse roughness length scale $k_N$. Typical Manning roughness values for bottom surfaces without vegetation range from 0.02 to 0.04 m$^{1/3}$/s. Conversion to $k_N$ via Bretschneider et al. (1986) gives a $k_N$ between 0 and 0.02 m for water depths between 0 and 3 m. This range is schematized by means of a uniform distribution with values between 0 and 0.02 m. The function to determine the increase in wave period $T_{m-1,0}$ is multiplied with a factor $f_T$ with mean value equal to 1.0 and standard deviation of 0.09, to account for the uncertainty of the predictive formula proposed in Hofland et al. (2017). They prescribe this standard deviation for a wave height to water depth ratio of approximately 0.5, which is often found on salt marshes due to depth-limitation of the wave height.

### 3.2.7. Vegetation properties

The most abundant plant species at the study location is *Elymus athericus*, a tall, thin and densely growing flexible grass. Characteristics of this species are taken from flume tests of Möller et al. (2014) (mean values $b_v = 1.30$ mm, $h_v = 700$ mm, $N_v = 1225$ stems/m$^2$). Three-point-bending tests of the same vegetation were performed by Rupprecht et al. (2017) to assess mechanical properties, and reanalyzed by Vuik et al. (2018) to determine the flexural strength (mean value $\sigma_{max} = 40$ MPa). Two types of standard deviations are of interest. Firstly, inter-sample variation, which characterizes differences in mean values within the marsh. And secondly, in-sample variation, which characterizes variation of the individual stems within the sample. The inter-sample variation is used in the probabilistic calculations to select representative values for wave attenuation, whereas the in-sample variation is used to compute a fraction of broken stems in each grid cell. In-sample variation is based on the standard deviations mentioned in Möller et al. (2014), and expressed in terms of coefficients of variation (CV) with respect to the mean values ($CV = \sigma/\mu$), see Appendix A. Inter-sample variation is based on variations between samples, taken from different locations on salt marshes along the coast of the province Friesland in the Netherlands, where extensive vegetation mapping and testing of mechanical properties was carried out in November 2016.

Apart from the vegetation characteristics, parameters have to be specified for the modeling of wave attenuation and stem breakage. For wave attenuation, a bulk drag coefficient $\tilde{C}_D = 0.22 \pm 0.05$ is based on the parametrization proposed in Möller et al. (2014), given the stem diameter of 1.3 mm and an orbital velocity of 1.0 m/s. Although information on the variation of bulk drag coefficients is missing, $CV(\tilde{C}_D) = 0.25$ is applied. For stem breakage, a theoretical value for the drag coefficient for cylinders in waves $C_D = 1.0$ is applied (Hu et al., 2014). The bulk drag coefficient $\tilde{C}_D$ is lower than the drag coefficient $C_D$, since $\tilde{C}_D$ includes the effects of swaying and leaning, which are not present in the description of wave attenuation by vegetation. For the skin friction coefficient $C_f$, a value of 0.01 is adopted from Luhar and Nepf (2011). Standard deviations of 0.25 for $C_D$ ($CV = 0.25$) and 0.005 for $C_f$ ($CV = 0.50$) are applied, to reflect the lack of knowledge on these parameters.

The reduction in stem height due to leaning $f_r = (h_v - h_{v,r})/h_v$ is based on observations in a wave flume by Rupprecht et al. (2017). For the tests just before the initiation of folding, a canopy height of 9 cm was observed, which leads to a reduction of $f_r = 0.87$. To determine a suitable standard deviation, a value of $h_{v,r} = 13$ cm is considered, which leads to a standard deviation in $f_r$ of 0.04. The parameter $A_c = 1.7$ was found in the calibration of the stem breakage model for *Spartina anglica*, and applied in the validation for *Elymus athericus* in Vuik et al. (2018). A standard deviation of 0.5 is applied to account for the uncertainty in the model predictions of the complicated process of stem breakage. This standard deviation is based on the differences in $A_c$ between the two plant species considered in Vuik et al. (2018). Finally, a height of broken stems $h_{v,br}$ is specified by means of a uniform distribution ranging from 2 to 8 mm. Stems are seen to fold and break near the bottom, both in the flume (Rupprecht et al., 2017) and in the field.

### 3.2.8. Boundary conditions for wind, water level and waves

Boundary conditions are represented by the parameters wind speed $U_{10}$, still water level $\zeta$, significant wave height $H_{m0}$ and mean wave period $T_{m-1,0}$. The probability distributions of these parameters represent the situation at the marsh edge of the salt marshes in the Dutch Wadden Sea, along the coast of the province of Groningen (Fig. 6).

First, a joint probability distribution for wind speed and water level is determined, based on a time series with 30 years of measured still water levels, wind directions and wind speeds. A peak-over-threshold analysis is performed to select storms for which the 97.5% percentile value for wind speed and/or water level is exceeded, during at least 6 h. Storms are selected with a wind direction at the peak water level within a sector of 45° around North-West (292.5–337.5 nautical degrees). Only storms from this wind sector generate high surge in the Wadden Sea (Fig. 6). Adding storms outside this sector does only result in more scatter, without significant influence on the marginal distribution for the water level. Since the data exhibits greater dependence in the positive tail than in the negative, a Gumbel copula (with parameter $\alpha = 2.24$) is chosen to describe the correlation structure. See e.g. Salvadori et al. (2014, 2015) and Sebastian et al. (2017) for recent applications of copula's in the field of coastal engineering. Two Generalized Extreme Value (GEV) distributions are fitted through the data, to obtain marginal distributions for wind speed and water level. A Poisson distribution (with parameter $\lambda = 6.4$) describes the number of storms per year in the selected wind sector. This set of distributions defines statistics per storm event.

Statistics per storm event are converted into statistics per year, by simulating 10,000 years of data via Monte Carlo sampling. For each year, a number of storms $N$ is sampled from the Poisson distribution, and $N$ random realizations of wind speed and water level are drawn from the Gumbel copula. From these $N$ realizations, the annual maximum still water level and corresponding wind speed are selected. This leads to a new data set, with 10,000 simulated annual maximum still water levels and corresponding wind speeds. Marginal GEV distributions are fitted through these new data, and the correlation between both variables is described by a Gaussian copula with $\rho = 0.43$, since no asymmetrical tail dependence is visible for the annual maximum values.

An existing database with the results of SWAN computations is deployed to determine wave conditions at the marsh edge. These SWAN computations were carried out to determine wave loads for the official assessment of the Dutch dikes surrounding the Wadden Sea (Groeneweg et al., 2010). 10,000 random data pairs with wind speed and water level are sampled from the Gaussian copula with $\rho = 0.43$. A wave height and wave period are coupled to these data pairs via 2D interpolation between the values in the database for the nearest wind direction (330°). The extreme values of the sampled wave parameters could well be described by Weibull type marginal distributions, and Gaussian correlation between the variables. Parameters of all distributions and correlation coefficients are included in Tables 9 and 10 in Appendix A. Some characteristic values from the marginal distributions are shown in Table 2.

Model uncertainty of the SWAN model was analyzed by Chbab and Groeneweg (2015), by comparing model results and measured wave conditions. Wave heights and wave periods are multiplied with a normally distributed model factor with a mean value (bias) and a standard deviation.

For wave impact on the outer slope, also the load duration is of importance, Eq. (14). Storms are selected from a time series, measured at a nearby measurement station at Eemshaven, deployed by Rijkswaterstaat. A mean value and standard deviation of the load duration have been determined for different values of the layer height $\Delta z$.

### 3.3. Definition of dependencies

Variables are assumed to be independent, except for situations with physical or statistical arguments for correlation. In the latter situation, Gaussian correlation between input variables is applied (section 2.6) for the following variables.

– dependence between wind, water level, wave height and wave period (see Section 3.2 and Table 10 in Appendix A)
– stem height $h_v$ is positively correlated with stem diameter $b_v$ in the *Elymus* samples ($\rho = 0.20$);
– thicker stems generally have a lower flexural strength $\sigma_{max}$ ($\rho = -0.33$);
– the correlation between stem height and flexural strength is weak ($\rho = -0.07$);
– full dependence of the bulk drag coefficient and drag coefficient is applied, because of many reasons for dependence between these parameters, such as a large frontal area due to many leaves ($\rho = 1.00$);
– flexural strength $\sigma_{br}$ and stiffness modulus $S_a$ of the asphalt did not display significant correlation for the 5 tests ($\rho = 0.01$). However, if one divergent test is excluded, a considerably higher correlation is found ($\rho = 0.46$). An additional calculation (not shown) with the latter correlation coefficient incorporated displayed lower failure probabilities ($\Delta\beta = 0.15 - 0.90$, with biggest influence for high quality asphalt). Nonetheless, the relative effect of a vegetated foreshore is nearly the same in both calculations ($\Delta\beta = 1.05 - 1.45$ for $\rho = 0.01$ versus $\Delta\beta = 0.99 - 1.55$ for $\rho = 0.46$).

**Table 2**
Characteristic values for boundary conditions.

| Boundary condition | Unit | Min | Max | |
|---|---|---|---|---|
| Spring tide | m MSL | −1.60 | 1.35 | |
| Wind direction | naut. deg. | 292.5 | 337.5 | |
| Exceedance frequency | 1/year | 1/10 | 1/100 | 1/1000 |
| Surge | m | 1.88 | 2.56 | 3.12 |
| Still water level | m MSL | 3.23 | 3.91 | 4.47 |
| Wind speed | m/s | 21.2 | 25.5 | 28.9 |
| Significant wave height | m | 0.90 | 1.26 | 1.54 |
| Mean wave period | s | 4.08 | 4.92 | 5.49 |

## 4. Results

### 4.1. Overview of simulations

Failure probabilities are computed for various system configurations, based on the salt marshes in the Dutch Wadden Sea. System components (dike, foreshore bathymetry, vegetation, vegetation stability), and the corresponding models and variables, are stepwise added to the simulations to assess their effect on the probability of failure. Table 3 explains which system components are included in the simulations. The reference case is a situation with only a dike, with a uniform foreshore at the level of the offshore tidal flats $z_0$. Next, a non-vegetated foreshore with the bathymetry of a salt marsh is considered. After that, vegetation is added, disregarding possible stem breakage. Finally, the model is completed by adding the stem breakage model and vegetation stability characteristics. A fraction of broken stems is computed in those simulations.

For each system configuration, a probabilistic (P) and deterministic (D) simulation is performed (Table 3). In the deterministic simulations, a standard deviation of 0 is assigned to variables that describe the foreshore, vegetation, and associated models. In the probabilistic computations, uncertainties in these parameters are included.

### 4.2. Probability of failure due to wave overtopping

An annual failure probability is computed for the different system configurations, considering erosion of the dike due to wave overtopping for three different crest levels (Fig. 9). Without a foreshore (i.e., foreshore at MSL), an annual failure probability of 1/18 is computed for a crest level of 4 m MSL (i.e., dike failure would occur every 18 year, on average). This probability reduces to 1/2200 for a 6 m MSL crest level, and to 1/1,500,000 for 8 m MSL. The ratio in dike volume (m³/m) between these three dikes is approximately 1:2:4. Corresponding reliability indices $\beta$ are 1.60, 3.32 and 4.83, respectively. Effects on the failure probability can best be expressed in terms of a change in reliability index ($\Delta\beta$), where a higher reliability index implies a lower failure probability, Eq. (8). Addition of a foreshore without vegetation leads to $\Delta\beta = 0.21$ (4 m MSL) up to 0.32 (8 m MSL). A foreshore with stable vegetation has a considerably higher effect: $\Delta\beta = 0.60$ (4 m MSL) up to 0.70 (8 m MSL). However, if also stem breakage is taken into account, the probability of failure approaches the situation of a non-vegetated foreshore due to severe breakage of vegetation, especially for the dikes of 6 MSL and 8 m MSL (Table 4). Under such conditions, wave attenuation by vegetation reduces to the influence of short, broken stems only. Fig. 9 also shows that the influence of uncertainties in foreshore bathymetry and wave model parameters is of minor importance, looking at the difference between a probabilistic (yellow bars) and deterministic description of the foreshore (gray bars underneath). Only for computations with stable vegetation, considerable differences are visible between the deterministic and probabilistic (green bars) simulations.

Now we consider the design points of the simulations (Table 4). The presence of a salt marsh leads to a shift in hydrodynamic conditions. Failure of a dike with foreshore occurs at higher water levels than without foreshore (i.e., foreshore at MSL). Waves are higher offshore, but lower at the dike. A distinct wave height reduction is visible for configurations with a shallow foreshore, due to energy dissipation by breaking and vegetation, whereas energy gain due to wind input can occur on a low foreshore. The overall effect of the foreshore on wave overtopping is reduced due to an increase in mean wave period $T_{m-1,0}$ over the foreshore. High waves lead to high fractions of broken stems for the configurations with dike crest levels at 6 and 8 m MSL. The orbital velocities for these waves ($u_{1/10} = 1.6$ m/s for $z_c = 8$ m MSL) are clearly higher than the critical velocity of the majority of the *Elymus* stems ($u_{crit} = 1.0 \pm 0.3$ m/s).

As an alternative interpretation of Fig. 9, a required crest level can be determined for a fixed target probability, using logarithmic interpolation.

**Table 3**
System components (rows), included in the 4 different simulations (columns), which are carried out in probabilistic (P) and deterministic (D) mode. System components are included via their mean value ('*') or its full probability distribution ('X').

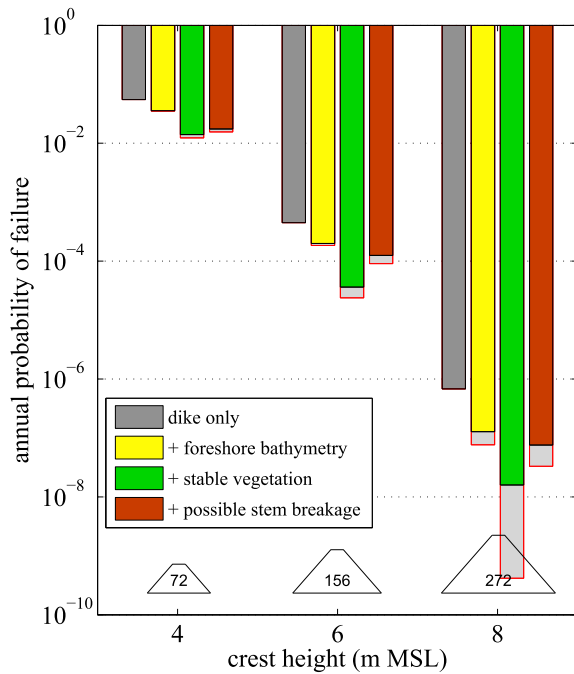| | dike only (foreshore at MSL) | | foreshore, no vegetation | | foreshore, stable vegetation | | foreshore, breakable vegetation | |
|---|---|---|---|---|---|---|---|---|
| | D | P | D | P | D | P | D | P |
| dike characteristics | X | X | X | X | X | X | X | X |
| wave load model | X | X | X | X | X | X | X | X |
| wave model | * | X | * | X | * | X | * | X |
| foreshore bathymetry | | | * | X | * | X | * | X |
| vegetation properties | | | | | * | X | * | X |
| vegetation model | | | | | * | X | * | X |
| stability properties | | | | | | | * | X |
| stability model | | | | | | | * | X |



**Fig. 9.** Probability of failure for the four different system configurations of Table 3, for three different dike crest levels. Computations with a probabilistic (colored bars) and deterministic (gray bars with red lines) description of the foreshore are shown (see Table 3). Dike sections are shown (vertical scale exaggerated), with the dike volume above mean sea level ($m^3/m$) inside. (For interpretation of the references to color in this figure legend, the reader is referred to the Web version of this article.)

For example, for a target annual failure probability of 1/1000, a crest level of 5.67 m MSL is required for a dike only (i.e., a dike with a foreshore at MSL). This required crest level reduces to 5.38 m MSL (non-vegetated foreshore), 4.89 m MSL (foreshore with stable vegetation) or 5.16 m MSL (foreshore with breakable vegetation). The difference in required crest level at this target probability equals 0.29 m, 0.78 m and 0.51 m, respectively. The corresponding reductions in required dike volume above MSL are 10%, 25% and 16%, assuming a crest width of 2 m and inner and outer slope angles of 1:4. If we neglect uncertainties on the foreshore, and work with mean values for all foreshore characteristics and model parameters, the differences in required crest level at 1/1000 are only slightly larger: 0.29 m, 0.86 m and 0.60 m, respectively. This confirms the aforementioned observation that uncertainties concerning the foreshore have less effect on the failure probability than uncertainties in boundary conditions, wave overtopping model, dike geometry and dike strength.

### 4.3. Relevance of uncertainties for wave overtopping

Fig. 10 shows how the relative contribution of system components to the failure probability, Eq. (10), is distributed over the different system components listed in Table 3: 'dike characteristics' (i.e., uncertainty in geometry and strength), 'wave load model' (i.e., the wave overtopping formulas), 'foreshore bathymetry', 'wave model', 'vegetation properties', 'vegetation model', 'vegetation stability properties' and 'vegetation stability model'. For example, the relative contribution of the system component 'vegetation properties' is equal to the sum of the $c_i$ of the variables stem density, stem height and stem diameter, see Appendix A. The first 3 bars in the figure show the relative contribution of the different system components for a 'dike only' system with mean crest levels of 4, 6 and 8 m MSL. The other groups of 3 bars belong to the system configurations that include a non-vegetated foreshore, a foreshore with stable vegetation, and a foreshore with breakable vegetation,

**Table 4**
Annual failure probabilities for different foreshore configurations and dike heights, with the hydrodynamic conditions in the corresponding design points.

| Foreshore configuration | $z_c$ | $\beta$ | $P_f$ | $\zeta$ | $H_{m0}$ (m) | | $T_{m-1,0}$ (s) | | $f_{br}$ |
|---|---|---|---|---|---|---|---|---|---|
| | (m MSL) | (−) | (−) | (m MSL) | in | out | in | out | (%) |
| dike only (foreshore at MSL) | 4 | 1.60 | $5.5 \cdot 10^{-2}$ | 3.38 | 1.00 | 1.08 | 4.1 | 4.1 | x |
| foreshore, no vegetation | | 1.80 | $3.6 \cdot 10^{-2}$ | 3.53 | 1.02 | 0.70 | 4.2 | 4.7 | x |
| foreshore, stable vegetation | | 2.20 | $1.4 \cdot 10^{-2}$ | 3.77 | 1.10 | 0.49 | 4.3 | 4.8 | 0% |
| foreshore, breakable vegetation | | 2.11 | $1.7 \cdot 10^{-2}$ | 3.63 | 1.07 | 0.59 | 4.2 | 4.7 | 55% |
| dike only (foreshore at MSL) | 6 | 3.32 | $4.5 \cdot 10^{-4}$ | 4.50 | 1.62 | 1.64 | 5.5 | 5.5 | x |
| foreshore, no vegetation | | 3.54 | $2.0 \cdot 10^{-4}$ | 4.70 | 1.62 | 1.20 | 5.5 | 6.0 | x |
| foreshore, stable vegetation | | 3.97 | $3.6 \cdot 10^{-5}$ | 4.82 | 1.69 | 1.10 | 5.4 | 5.9 | 0% |
| foreshore, breakable vegetation | | 3.66 | $1.3 \cdot 10^{-4}$ | 4.77 | 1.66 | 1.15 | 5.4 | 5.9 | 87% |
| dike only (foreshore at MSL) | 8 | 4.83 | $6.8 \cdot 10^{-7}$ | 5.39 | 2.17 | 2.07 | 6.7 | 6.7 | x |
| foreshore, no vegetation | | 5.15 | $1.3 \cdot 10^{-7}$ | 5.64 | 2.20 | 1.68 | 6.4 | 6.9 | x |
| foreshore, stable vegetation | | 5.53 | $1.6 \cdot 10^{-8}$ | 5.75 | 2.25 | 1.61 | 6.5 | 7.0 | 0% |
| foreshore, breakable vegetation | | 5.25 | $7.6 \cdot 10^{-8}$ | 5.70 | 2.26 | 1.65 | 6.4 | 6.9 | 96% |
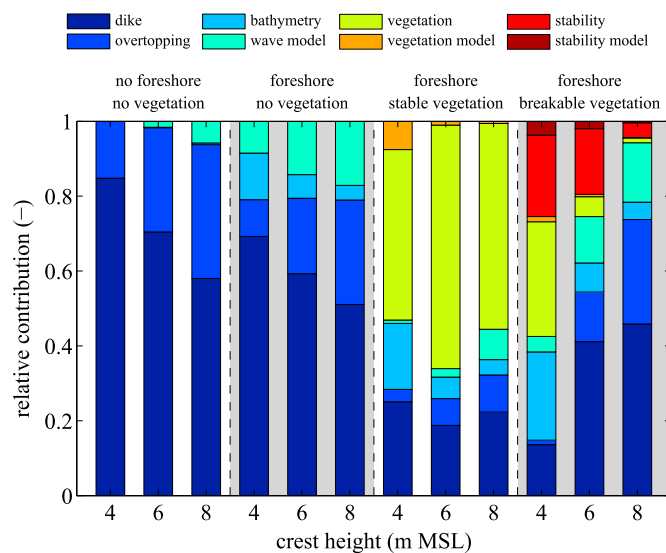
**Fig. 10.** The relative contribution of the different system components from Appendix A to the probability of failure due to wave overtopping. System configuration are, from left to right: a dike without foreshore, a non-vegetated foreshore, a foreshore with stable vegetation, and a foreshore with breakable vegetation. The three bars per system configuration belong to the three different crest levels in the computations (4, 6 and 8 m MSL).

respectively.

The figure shows that uncertainties in dike geometry and dike strength dominate the probability of failure for a dike only (apart from the boundary conditions). Uncertainty in wave overtopping discharge (especially parameter $b_1$) gains relative importance with increasing dike height. This is partly due to an increase of its importance factor ($\alpha = 0.05$ for 4 m MSL and 0.16 for 8 m MSL), and partly due to a decrease of the importance factor for the uncertainty ($\sigma = 0.10$ m) in dike crest level ($\alpha = 0.11$ for 4 m MSL and 0.08 for 8 m MSL). If a non-vegetated foreshore is added to the system, the components 'foreshore bathymetry' and 'wave model' come into play. Uncertainties in foreshore bathymetry (especially in the foreshore height $z_{fs}$) are mainly important for a low dike, whereas the influences of uncertainties in wave model parameters (especially the breaker parameter $\gamma$) increase with increasing dike height. In general, uncertainties in system characteristics are more important for low dikes and high failure probabilities. Model uncertainties show the opposite trend, with higher importance for high dikes with low failure probabilities.

The right half of the figure deals with vegetated foreshores. If the vegetation can be considered as fully stable, vegetation characteristics (especially the stem density $N_v$, due to its high spatial variation) and vegetation model (i.e., the bulk drag coefficient $\tilde{C}_D$) dominate the uncertainty. However, most *Elymus* stems will break under these conditions. Therefore, addition of the stem breakage model changes the dominant uncertainties drastically. The influence of uncertainty in bulk drag coefficient (vegetation model) diminishes, as it does not only increase wave attenuation, but also stem breakage, due to the correlation between $C_D$ and $\tilde{C}_D$. Uncertainty in vegetation stability has the largest contribution for the system with a low dike (4 m MSL). Also vegetation characteristics are still important for this configuration. Stem density acts as a strength variable ($\alpha > 0$), whereas stem height acts as a load variable ($\alpha < 0$). This is because of the lower stability of longer stems, which dominates over the effect on wave attenuation. For the high dike (8 m MSL), uncertainty in the stem breakage process diminishes, as almost all stems will undoubtedly break. The distribution of relative contributions strongly resembles the situation of the non-vegetated foreshore.

## 4.4. Sensitivity analysis for wave overtopping

Different variations are applied with respect to the system characteristics of the base case, listed in Appendix A, to test the response of the failure probability to different choices concerning important system characteristics. In the panels below, the effect of a vegetated foreshore (with breakable vegetation) is shown along different gradients, in the panels a–f:

(a) marsh width (base case: 300 m),
(b) tolerable overtopping discharge (base case: 63 l/s/m),
(c) flexural strength of vegetation (base case: 40 MPa),
(d) correlation between wind and water level (base case: $\rho = 0.43$),
(e) offshore wave height,
(f) sea level rise (base case: 0 m).

Effects can best be expressed in terms of the reliability index $\beta$, which is directly related to the failure probability via Eq. (8).

First, variations in foreshore width are applied ($B_{fs} = 100$ m, 300 m and 900 m), see Fig. 11, panel (a). Wider foreshores lead to lower failure probabilities, especially if the vegetation remains stable (low dike, 4 m MSL), since wave attenuation by vegetation is more dependent on marsh width than, for example, wave breaking. Logically, uncertainty in marsh width is more important for small marshes, for equal standard deviation of 50 m. However, even for the 100 m wide foreshore, the importance factor $\alpha$ for the uncertainty in marsh width (0.07–0.09, depending on crest level) is still smaller than for example the importance factor for the tolerable overtopping discharge (0.09–0.19).

The mean value of 63 l/s/m for the tolerable overtopping discharge $q_{max}$ is valid for healthy grass covers on clay. Dikes with a damaged grass cover, or a sandy subsoil, are characterized by a significantly lower erosion resistance. Panel (b) compares the failure probabilities for values of 63 (base case) and 6.3 l/s/m (factor 10 lower). Also the standard deviation is divided by 10. The effect of a vegetated foreshore compared to a dike only system is slightly larger ($\Delta\beta = 0.46 - 0.74$) for the lower tolerable overtopping discharge compared to the base case ($\Delta\beta = 0.34 - 0.51$). This means that vegetated foreshores are more effective for dikes with lower overtopping resistance.

Next, the effect of vegetation strength $\sigma_{max}$ is investigated. Panel (c) contains failure probabilities for the base case (medium strength), strength values (both $\mu$ and $\sigma$) divided by 2 (low strength), values multiplied by 2 (high strength), and fully stable vegetation. The vegetation in the high strength simulation behaves as fully stable for the low dike (only 8% breakage, against 48% in the base case). The difference between strength scenarios decreases for the medium dike and high dike, as the fractions of broken stems become 53% and 87%, respectively, versus 89% and 96% in the base case. A factor 2 in flexural strength is equivalent to a factor $\sqrt{2}$ in stem height or stem diameter, see Eq. (2), so shorter or thicker stems would display comparable behavior (disregarding correlation effects).

Panel (d) shows the system behavior when correlation between wind speed and water level is weaker ($\rho = 0.10$) or stronger ($\rho = 0.90$) compared to the base case ($\rho = 0.43$). The corresponding dependence of wave conditions on wind speed and water level is determined in the same way as for the base case, see section 3.2. A lower correlation between wind and water level may occur if variations in river discharge or storage volume in a lake are more relevant. Lower correlation leads to higher reliability indices. However, also the effect of a vegetated foreshore (the length of the lines) becomes smaller. This is because the dominant loading conditions can shift to a situation with moderate waves combined with high water depths, for which the interaction between waves and the vegetated bottom surface is lower. Such a shift is more likely in case of low correlation.

Panels (e) and (f) show the effect of offshore wave height and sea level rise, which can both be induced by climate change. For the offshore wave
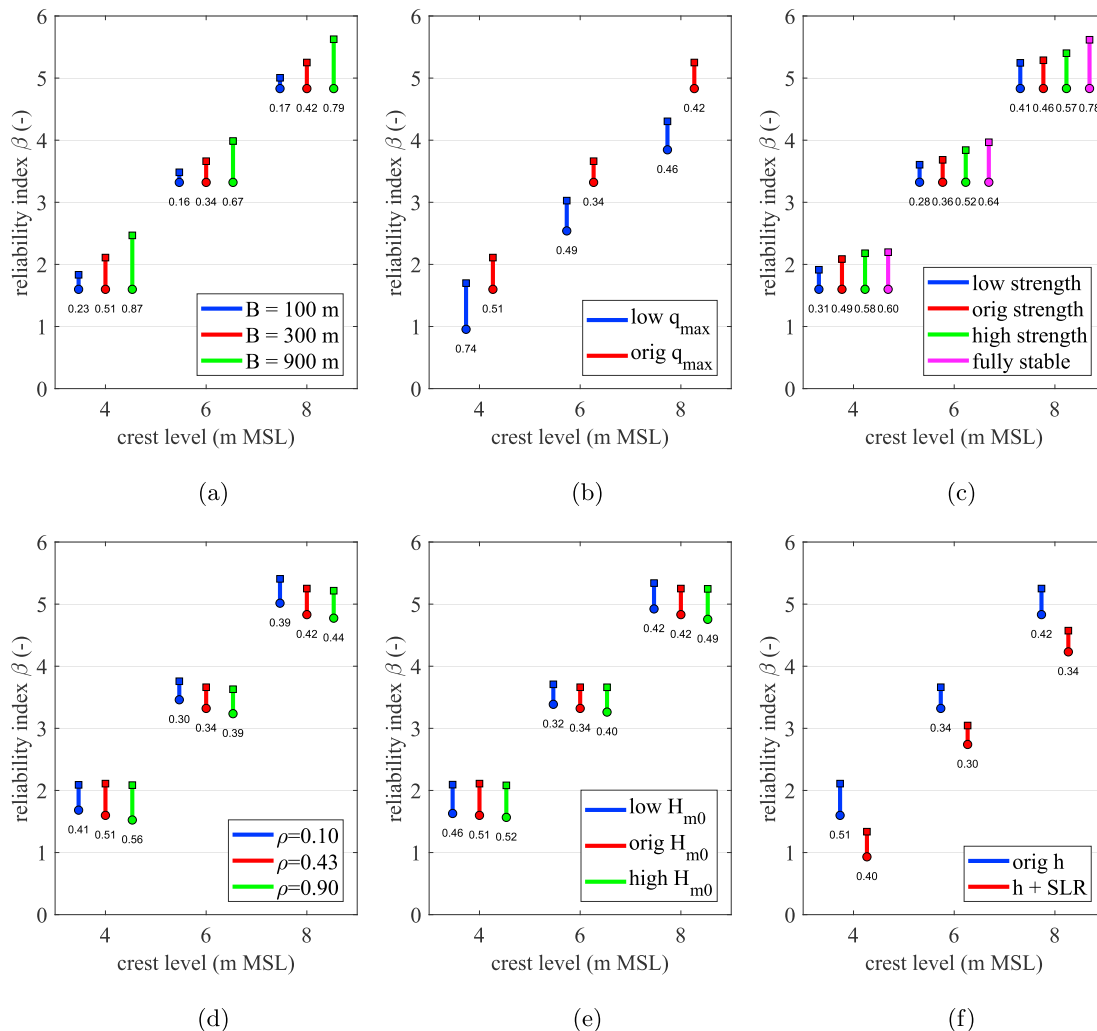
**Fig. 11.** Sensitivity of the reliability index $\beta$ to different values of the marsh width (panel a), tolerable overtopping discharge (b), flexural strength of the vegetation (c), correlation coefficient between wind, water level and wave height (d), offshore wave height (e) and sea level rise (f). Circular markers at the lower end of the lines concern the dike only system; the square markers at the upper end of the lines concern the system with a vegetated foreshore. The numbers below the lines show the differences in $\beta$ between both systems (i.e., the length of the lines).

height, the shape parameter of the Weibull distribution is 2.05 (base case), 2.26 (lower wave height) or 1.85 (higher wave height). Differences between offshore wave height reduce due to the presence of a foreshore, which makes a foreshore slightly more efficient in case of high offshore waves (panel e), which is in line with van Wesenbeeck et al. (2017). For sea level rise, a scenario is added with an increase in still water level of 0.50 m with respect to the original water level statistics (panel f). Without morphological adjustment, sea level rise will also cause an increase in wave heights (Arns et al., 2017). Therefore, the incoming wave height is amplified as well, by applying a wave height to water depth ratio ($H_{m0}/(\zeta - z_0)$) identical to the situation without sea level rise. The computations show that the effect of a vegetated foreshore on $\beta$ decreases in case of sea level rise.

### 4.5. Probability of failure due to wave impact on revetments

Fig. 12 shows failure probabilities for a medium quality (A1, $\sigma_{br} = 3$ MPa, $c_{sub} = 60$ N/m$^3$) and low quality asphalt revetment (A2, $\sigma_{br} = 1.5$ MPa, $c_{sub} = 30$ N/m$^3$). For medium quality (A1), the presence of a salt marsh leads to an increase of the reliability index $\beta$ by 1.04 (foreshore without vegetation), 1.21 (foreshore with breakable vegetation) or 1.40 (foreshore with stable vegetation). These differences in $\beta$ are higher for

low quality (A2): 1.13, 1.45 and 1.75, respectively. According to the model, 90 (A2) to 96% (A1) of the vegetation breaks. Effects of foreshores on reliability indices, and thus on failure probabilities, are considerably higher than for failure due to wave overtopping.

According to the implemented models for asphalt and grass, a high quality grass cover on a 1:8 slope has a strength comparable to low quality asphalt (A2) on a 1:4 slope. Presence of a salt marsh leads to an increase in $\beta$ of 1.18 (foreshore without vegetation), 1.45 (foreshore with breakable vegetation) or 1.76 (foreshore with stable vegetation), which is similar to the results for an asphalt revetment.

### 4.6. Relevance of uncertainties for wave impact on revetments

Generically speaking, the distribution of uncertainties for wave impact on revetments (Fig. 13) is similar to the case of failure due to wave overtopping (Fig. 10). The main difference is the contribution of uncertainty in dike strength. For wave overtopping, the overall uncertainty is dominated by the boundary conditions only, with a minor contribution ($\sum \alpha_i^2 \approx 0.02 - 0.05$) of dike characteristics and strength. For asphalt revetments, uncertainty in asphalt properties is of significant importance ($\sum \alpha_i^2 \approx 0.30 - 0.55$), which implies that failure of asphalt revetments most likely occurs due to a moderate storm combined with a pessimistic
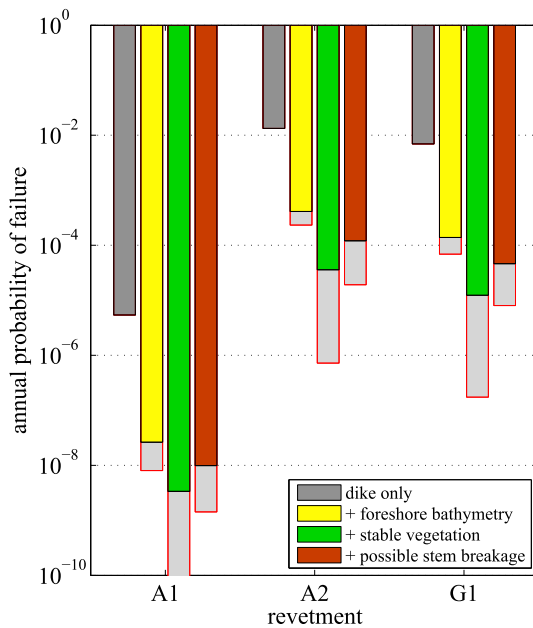
**Fig. 12.** Probability of failure due to wave impact on revetments for a revetment of medium strength (A1) and low strength asphalt on a 1:4 slope (A2), and closed grass sods on a 1:8 slope (G1). Computations with a probabilistic (colored bars) and deterministic (gray bars with red lines) description of the foreshore are shown (see Table 3). (For interpretation of the references to color in this figure legend, the reader is referred to the Web version of this article.)
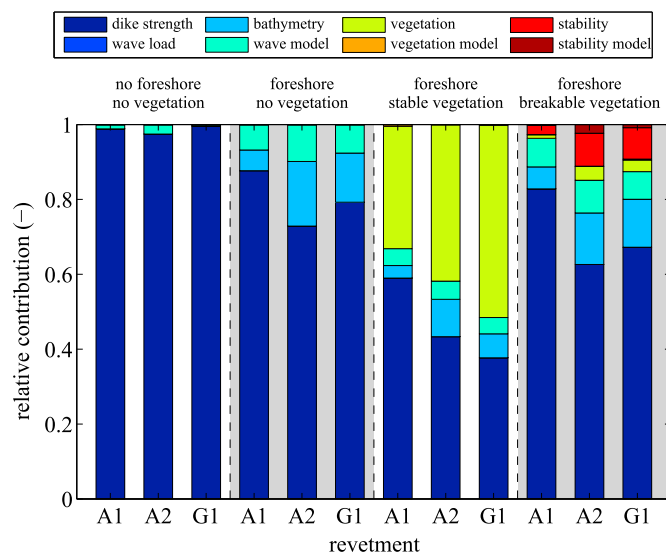


**Fig. 13.** The relative contribution of the different system components from Appendix A to the probability of failure due to wave impact on revetments. System configuration are, from left to right: a dike with no foreshore, a non-vegetated foreshore, a foreshore with stable vegetation, and a foreshore with breakable vegetation. The three bars per system configuration belong to a revetment of medium strength (A1) and low strength asphalt on a 1:4 slope (A2), and closed grass sods on a 1:8 slope (G1).

scenario for the asphalt strength.

Since strong waves are required to break medium strength asphalt (A1), most vegetation will break, and the distribution of uncertainties of a foreshore with breakable vegetation strongly resembles the case of a foreshore without vegetation. For low strength asphalt (A2) and closed grass sods (G1), the uncertainty in vegetation stability is more relevant. However, considering the *Elymus* vegetation as fully stable is not realistic in both cases.

## 5. Discussion

Uncertainties of nature-based flood defenses are not yet systematically evaluated. This paper is a first assessment of uncertainties surrounding dikes with a grass or asphalt cover combined with a vegetated salt marsh foreshore. It shows how different foreshore configurations affect failure probabilities of hybrid flood defenses, and how uncertainties in different system components contribute to this probability of failure.

### 5.1. Discussion of methods

The model framework consists of different connected modules, each with its own limitations. Formulas for dike failure due to wave overtopping or wave impact on asphalt and grass covers are simplified descriptions of complicated processes, as well as the description of wave attenuation by flexible vegetation that is prone to stem breakage. Marsh edge erosion is an example of a process that is simply taken into account via a standard deviation on the marsh width. There may be room for improvement in all these models. However, this is outside the scope of the current study, which focuses on integrating different models into one probabilistic calculation framework. The similarity in results for three independent models for dike failure mechanisms gives confidence in more general validity of the main conclusions in this paper.

Results are based on a specific site with an exposed dike and salt marsh in the Dutch Wadden Sea, with vegetation characteristics of *Elymus athericus*. Choices regarding probability distributions are mostly based on field and flume observations, which results in a realistic case study. Some choices are generically valid, other choices will be more site-specific. The sensitivity analysis shows that trends and conclusions are more broadly applicable than the specific location only. Regardless, the probabilistic framework can be applied to any other location where a dike is loaded by waves, and bordered by a vegetated foreshore. Examples are wetlands surrounding the Mississippi delta (USA) and hybrid flood defenses with mangroves and levees in the Mekong delta (Vietnam).

The First Order Reliability Method (FORM) is a relatively simple probabilistic method, which is able to compute a failure probability in 20–40 iterations. Within each iteration, 2 computations are performed for each stochastic variable, since 2-sided derivatives are applied. Computation times are approximately 1 min per failure probability on one CPU. Only computations with stem breakage take longer (ca. 10 min), since internal sampling from distributions is involved to determine a fraction of broken stems. Alternative probabilistic methods, such as Monte Carlo, Importance Sampling or Numerical Integration require considerably more computational time. We did not experience convergence problems of the iterative FORM computations, as long as continuous functions were used, and an initial design point was specified for which non-zero partial derivatives could be calculated.

### 5.2. Discussion of results

Presence of a salt marsh foreshore reduces the failure probability of the dike in behind, compared to a situation with a foreshore around mean sea level. This reduction is caused by depth-induced wave breaking, bottom friction and wave attenuation by vegetation. Stem breakage and an increase in mean wave period $T_{m-1,0}$ are factors that may reduce the efficiency of a vegetated foreshore. The reduction does not only apply to conditions with low water levels, since a system is considered here with positive correlation between wind speed, water level and wave height, characterized by depth-limitation of the wave height. An increase in water level will be accompanied with an increase in wave height. The ratio between wave height and water depth determines the efficiency of a vegetated foreshore, not the water depth only (Vuik et al., 2016). The additional wave damping effect of vegetation on the salt marsh decreases with increasing water depth and wave height, as more stems will break.

The reduction in probability of failure due to wave impact on asphalt revetments or grass covers is more pronounced than for failure due to wave overtopping. The reason is that revetments can already be heavily impacted by waves at relatively low water levels. An increased water level is only needed to obtain a water depth for which high waves can reach the dike. With a foreshore at 0 m MSL, high waves can already damage the lower part of the revetment at a water level of approximately 4 m MSL. When a foreshore is present at 1.7 m MSL, such high waves can only reach the dike for higher water levels, with a much lower likelihood. This directly affects the probability of revetment failure. In contrast, severe wave overtopping and subsequent erosion requires high water levels, close to the dike crest level. The relative difference in water depth between situations with foreshores at 0 and 1.7 m MSL is smaller in that case.

This paper shows that the total relative contribution of uncertainties concerning the vegetated foreshore is generally smaller than the contribution of uncertainties related to dike geometry and strength. This seems counter-intuitive, since especially vegetation characteristics are characterized by a high spatial and temporal variability. However, the probabilistic computations shed light on the relevance of such uncertainties for failure of hybrid flood defenses. Uncertainty in dike strength is still dominant in most cases. This finding allays concerns about a lack of certainty with respect to this kind of solutions (Bouma et al., 2014), on short time scales. This holds for both dike failure mechanisms that were considered in this paper: erosion of the crest and rear slope due to wave overtopping and erosion of the outer slope revetment due to direct wave impact.

The relevance of different uncertainties depends on the protection level. In the application shown in this paper, vegetation and the related uncertainties are only relevant for the low dike. Most vegetation will withstand the wave forcing, since relatively low waves already lead to overtopping of the dike. The amount of standing vegetation strongly depends on the stability characteristics. Also uncertainties in initial vegetation state (stem diameter, height and density) are important. These characteristics lose importance with increasing dike height and protection level. Eventually, for a very high dike, which should withstand high waves, it is very likely that almost all vegetation will break. It is not reasonable to take into account wave attenuation by vegetation, while disregarding the threshold of stem breakage. Wave forces that lead to failure of the dike are too strong for the vegetation, and the distribution of relevant uncertainties is very similar to the situation of a dike with a non-vegetated foreshore.

Flood defenses which provide a relatively low protection level are found in many countries in the world (Scussolini et al., 2016). These countries are confronted with other relevant uncertainties than countries with a high protection level (Fig. 14). This finding can be used to make recommendations for future research. Inherent uncertainty and statistical uncertainty (section 2.7) concerning the state of the foreshore and vegetation are especially important for low dikes with low strength. Monitoring and predicting the variability of the foreshore and vegetation is very important in such conditions, as well as restriction of the variability by management, for example by grazing, permeable dams or marsh edge protection. Research and measurements will decrease knowledge uncertainty, and will strongly affect failure probabilities.

In countries with high and strong dikes, uncertainty in vegetation characteristics and foreshore bathymetry is less important (Fig. 14). This leads to a paradox: in countries with a high protection level, there is often a lot of data available concerning the foreshore and vegetation, while the need for these detailed data is relatively low. Foreshore geometry is more relevant than the vegetation, because of expected stem breakage in design conditions. Given an initial foreshore state, the overall uncertainty is restricted to the severity of storm conditions (mostly beyond the measured range), and to the dike strength. Therefore, a simple description of foreshore characteristics and processes suffices for high and strong dikes. Further, research regarding the protective value of vegetated foreshores should focus on morphological development, including
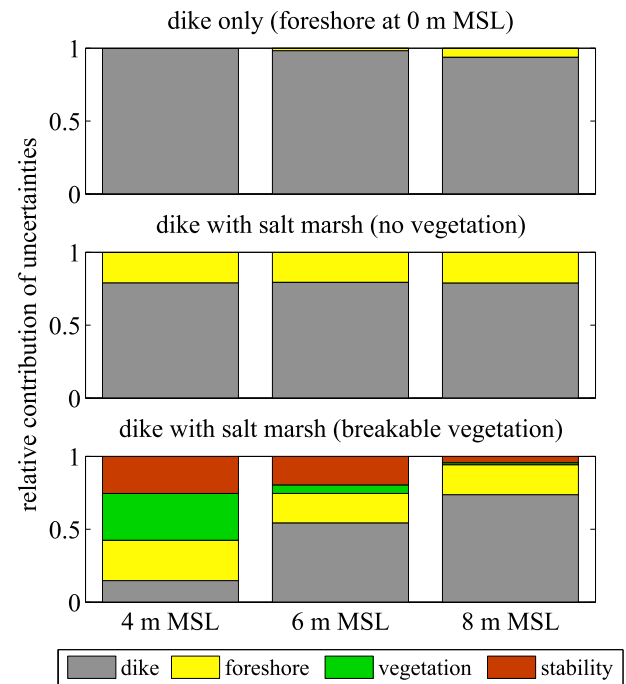
**Fig. 14.** The relative contribution of different uncertainties to the probability of failure due to wave overtopping. Uncertainties are subdivided into (1) dike (geometry, strength and overtopping model), (2) foreshore (geometry and wave model), (3) vegetation (characteristics and model parameters) and (4) vegetation stability (characteristics and model parameters). Contributions are shown for different foreshore configurations (three panels) and different crest levels (horizontal axes).

interactions with vegetation. While the direct role of vegetation under design conditions is limited, it does play an important indirect role in the medium to long term via bio-geomorphological interactions. Vegetation affects geomorphology via wave attenuation under moderate conditions (Möller et al., 2014), subsequent sediment trapping (Mudd et al., 2010), and stabilization of the salt marsh platform with its root systems (Francalanci et al., 2013; Lo et al., 2017).

Nature-based solutions for flood risk reduction are supposed to reduce the effect of climate change (Kirwan and Megonigal, 2013). This can partly be attributed to the aforementioned sediment trapping capacity, which makes that the foreshore can keep pace with sea level rise. This paper confirms that accretion on the foreshore is required to retain its efficiency. Further, higher offshore waves lead to a greater effect of foreshores on the failure probability, which implies that the impact of increasing storminess (Jones et al., 2012) will be lower if a foreshore is present.

### 5.3. Added value of a probabilistic approach

Application of a probabilistic approach gives insights in the absolute and relative importance of different uncertainties for flood risk reduction. Many parameters are needed to describe the characteristics and behavior of the hydrodynamics, dike, foreshore and vegetation. It is highly unlikely that unfavorable values for all those parameters occur simultaneously. Accumulation of conservative estimates would lead to an over-conservative design, which should be avoided. This can best be illustrated using a simple example with 2 parameters. We combine a water level with an annual probability of exceedance of 1% (once every 100 years, on average) with a conservatively chosen low bulk drag coefficient with a probability of non-exceedance of only 1%. This combination has a joint annual probability of occurrence of only 0.01% (assuming independence). Probably, the combination of a water level with an annual probability of exceedance of 0.01% (once every 10,000

years, on average) and the mean value of the bulk drag coefficient will lead to a worse situation. Both combinations have the same joint probability of occurrence. There is a need for a method that decides which variables should be chosen conservatively, and which variables may be chosen close to the expected value. The probabilistic method FORM, which was applied in this paper, provides such guidance in the form of design points.

## 6. Conclusions

This paper has investigated the probability of failure of a hybrid flood defense, which consists of a dike accompanied with a vegetated foreshore. An integrated modeling framework was developed, combining characteristics and model descriptions of the hydrodynamics, dike strength, foreshore bathymetry and vegetation. Probability distributions were based on field and flume observations. The probabilistic method FORM was applied to determine which uncertainties are most influential, and to compute the overall probability of failure of the dike-foreshore system. In this way, a hybrid flood defense can be assessed according to the same state-of-the-art standards as a standalone dike.

Two wave-driven failure mechanisms were considered: failure due to wave overtopping and failure due to wave impact on dike slope revetments. Vegetated foreshores cause a reduction in dike failure probability, which is caused by wave breaking, bottom friction and wave attenuation by vegetation. The effect of foreshores on wave impact on revetments is larger than their effect on wave overtopping, since waves are able to damage revetments already at moderate water depths, for which differences in foreshore configuration have a relatively high impact. Wave attenuation by vegetation has the highest effect on failure probabilities at low protection levels. This effect will become marginal if a high protection level is required. The flood defense should then be able to withstand high waves, which lead to stem breakage of most vegetation.

The effect of a vegetated foreshore on the probability of failure due to wave overtopping.

– increases with foreshore width,
– decreases with overtopping resistance of the dike,
– increases with vegetation strength,
– increases with increasing dependence between wind, water level and wave height,
– increases with offshore wave height,
– and decreases with sea level rise, without change in foreshore elevation.

The model provides insights into the relative contribution of various uncertainties to the failure probabilities. The relevance of different uncertainties depends on system configuration and protection level. For low dikes, most vegetation will withstand the wave forces under design conditions, and uncertainties in vegetation characteristics and behavior strongly influence the probability of failure. For high dikes, the overall short-term uncertainty is restricted to the storm conditions and dike strength. The foreshore causes wave energy dissipation by depth-induced wave breaking on the salt marsh platform.

Hybrid flood defenses can now be assessed according to the state-of-the-art standards based on failure probabilities, in which both uncertainties in load and strength are considered. Different sources of uncertainties can be compared, involved in hydraulic loads, dike geometry and strength, and characteristics of the vegetated foreshore. This enables the assessment of nature-based solutions as an alternative to more traditional engineering solutions.

## Acknowledgements

## Appendix A. Overview of probability distributions

The tables in this Appendix summarize all parameters and probability distributions used in the calculations. The following abbreviations are used. For nature of uncertainty: inherent (I), statistical (S) and/or model uncertainty (M); for location of uncertainty: boundary conditions (B), foreshore (F), vegetation (V), dike (D); for distribution type: normal (N), log-normal (L), uniform (U), Weibull (W), Generalized Extreme Value (G), deterministic (D).

**Table 5**
Parameters for dike strength (overtopping, asphalt, grass).

| Variable | Symbol | Units | Nature | Location | Distribution | Parameters |
|---|---|---|---|---|---|---|
| Dike crest level | $z_c$ | m MSL | S | D | N | $\mu$, 0.1 |
| Dike slope angle | $\alpha_d$ | deg. | S | D | N | 1/4, 1/80 |
| Tolerable overtopping discharge | $q_{max}$ | $ls^{-1}m^{-1}$ | I,S | D | N | 63, 19 |
| Flexural strength asphalt, A1 | $\sigma_{br}$ | MPa | I,S | D | L | 3.0, 0.90 |
| Flexural strength asphalt, A2 | $\sigma_{br}$ | MPa | I,S | D | L | 1.5, 0.45 |
| Modulus of subsoil reaction, A1 | $c_{sub}$ | N/m³ | S | D | L | 60, 12 |
| Modulus of subsoil reaction, A2 | $c_{sub}$ | N/m³ | S | D | L | 30, 6 |
| Thickness asphalt layer | $d_a$ | m | S | D | L | 0.25, 0.025 |
| Stiffness modulus asphalt | $S_a$ | MPa | I,S | D | L | 8000, 2400 |
| Poisson's ratio of asphalt | $\nu$ | – | I,S | D | D | 0.35 |
| Fatigue parameter asphalt | $V_\alpha$ | – | S | D | D | 0.5 |
| Fatigue parameter asphalt | $V_\beta$ | – | S | D | D | 4.8 |
| Parameter grass strength | $C_a$ | m | I,S | D | L | 1.82, 0.62 |
| Parameter grass strength | $C_b$ | 1/hr | I,S | D | D | −0.035 |
| Parameter grass strength | $C_c$ | m | I,S | D | D | 0.25 |
| Fraction of sand in clay | $f_{sand}$ | – | S | D | D | 0.35 |
| Thickness clay layer with roots | $d_{tot}$ | – | S | D | N | 0.50, 0.10 |

**Table 6**
Parameters for wave load model (overtopping, grass).

| Variable | Symbol | Units | Nature | Location | Distribution | Parameters |
|---|---|---|---|---|---|---|
| Parameter wave overtopping | $a_1$ | – | M | D | N | 0.023, 0.003 |
| Parameter wave overtopping | $b_1$ | – | M | D | N | 2.70, 0.20 |
| Parameter wave overtopping | $a_2$ | – | M | D | N | 0.09, 0.0135 |
| Parameter wave overtopping | $b_2$ | – | M | D | N | 1.50, 0.15 |
| Parameter wave overtopping | $a_3$ | – | M | D | N | −0.79, 0.29 |
| Factor slope angle effect | $r_\alpha$ | – | M | D | N | 1.51, 0.11 |

**Table 7**
Parameters for foreshore bathymetry and wave model.

| Variable | Symbol | Units | Nature | Location | Distribution | Parameters |
|---|---|---|---|---|---|---|
| Foreshore width | $B_{fs}$ | m | S | F | N | 300, 50 |
| Foreshore elevation | $z_{fs}$ | m MSL | S | F | N | 1.7, 0.2 |
| Foreshore slope angle | $\alpha_{fs}$ | deg. | S | F | D | 1/100 |
| Offshore bed level | $z_0$ | m MSL | S | F | D | 0.0 |
| Breaker parameter | $\gamma$ | – | M | F | N | $\mu$, 0.05 |
| Roughness length scale | $k_N$ | m | M | F | U | 0, 0.02 |
| Multiplier to increase $T_{m-1,0}$ | $f_T$ | – | M | F | N | 1.00, 0.09 |

**Table 8**
Parameters for vegetation, vegetation stability, and model parameters.

| Variable | Symbol | Units | Nature | Location | Distribution | Parameters |
|---|---|---|---|---|---|---|
| Stem height | $h_v$ | mm | I,S | V | N | 0.70, 0.05 |
| Stem diameter | $b_v$ | mm | I,S | V | N | 1.30, 0.13 |
| Stem density | $N_v$ | stems/m$^2$ | I,S | V | N | 1225, 575 |
| Stem flexural strength | $\sigma_{max}$ | MPa | I,S | V | N | 40, 12 |
| Variation of $h_v$ | CV($h_v$) | – | I,S | V | N | 0.02, 0.01 |
| Variation of $b_v$ | CV($b_v$) | – | I,S | V | N | 0.23, 0.05 |
| Variation of $\sigma_{max}$ | CV($\sigma_{max}$) | – | I,S | V | N | 0.70, 0.12 |
| Reduction factor for leaning | $f_r$ | – | S | V | N | 0.87, 0.04 |
| Height of broken stems | $h_{v,br}$ | mm | S | V | U | 0.02, 0.08 |
| Bulk drag coefficient | $\bar{C}_D$ | – | M | V | N | 0.22, 0.05 |
| Drag coefficient | $C_D$ | – | M | V | N | 1.00, 0.25 |
| Friction coefficient | $C_f$ | – | M | V | L | 0.010, 0.005 |
| Correction factor stem breakage | $A_c$ | – | M | V | N | 1.7, 0.5 |

**Table 9**
Boundary conditions (wind, water level, waves).

| Variable | Symbol | Units | Nature | Location | Distribution | Parameters |
|---|---|---|---|---|---|---|
| Wind speed | $U_{10}$ | m/s | I | B | W | 19.1, 3.00 |
| Still water level | $\zeta$ | m MSL | I | B | G | 0.42, 2.67, −0.09 |
| Significant wave height | $H_{m0}$ | m | I | B | W | 0.90, 2.50 |
| | | | M | B | N | 0.99, 0.19 |
| Mean wave period | $T_{m-1,0}$ | s | I | B | D | $s_0 = 0.08$ |
| | | | M | B | N | 0.96, 0.11 |
| Wave impact zone below $\zeta$ | $\Delta z$ | m | I | B | D | 1.0 |
| Load duration within $\Delta z$ | $t_{load}$ | hrs | I | B | N | 4.97, 0.68 |

**Table 10**
Pearson correlation coefficients for Gaussian dependence between boundary conditions.

| Variable | $U_{10}$ | $\zeta$ | $H_{m0}$ | $T_{m-1,0}$ |
|---|---|---|---|---|
| $U_{10}$ | 1.00 | 0.43 | 0.76 | 0.79 |
| $\zeta$ | 0.43 | 1.00 | 0.89 | 0.85 |
| $H_{m0}$ | 0.76 | 0.89 | 1.00 | 0.99 |
| $T_{m-1,0}$ | 0.79 | 0.85 | 0.99 | 1.00 |

## Appendix B. Failure due to wave impact on grass covers

This appendix summarizes the formulas describing dike failure due to wave impact on grass covers, and its implementation into a limit state function. Equations for the time required to erode the grass and clay layer are based on De Waal and Van Hoven (2015). Erosion of a grass cover starts at a certain threshold wave height $c_c$ (m), and increases with $H_{m0}$, depending on the empirical parameters $c_a$ (m) and $c_b$ (1/hr). This relationship reads

$$t_{top} = f_{\alpha_d} 1/c_b \ln\left[\frac{\max((H_{m0} - c_c); 0)}{c_a}\right]. \tag{11}$$

The time required to erode the clay layer underneath the grass cover follows from

$$t_{sub} = f_{\alpha_d}\frac{\max((d_{tot} - 0.2); 0)}{c_d(1/3)^{1.5}\max((H_{m0} - 0.5); 0)}, \tag{12}$$

in which $d_{tot}$ is the layer thickness of the clay layer, including the top layer with grass roots, and $c_d$ is a constant, depending on the sand fraction $f_{sand}$ ($c_d = 1.1 + 8\max(f_{sand} - 0.7; 0)$). Discontinuities in the functions may lead to instability of the probabilistic computations. Therefore, expressions of the form $\max(x - x_0); 0)$ are replaced by a continuous hinge function ($\max((x - x0); 0) = \delta\ln[1 + \exp((x - x0))/\delta]$), where the scale parameter $\delta$ is in the order of 0.01–0.1, depending on the magnitude of $x$. Kruse (2010) has studied the effect of other slope angles. Based on the differences in erosion duration for 1:3 slopes and 1:6 slopes, a linear correction factor for the slope angle is developed:

$$f_{\alpha_d} = \frac{(r_\alpha - 1)/3}{\tan\alpha_d} + 2 - r_\alpha, \tag{13}$$

where the ratio $r_\alpha$ between 1:6 and 1:3 slopes is 1.51 on average, with a standard deviation of 0.11.The load duration $t_{load}$ is defined as the duration (hrs) of the period in which the water level is between the peak still water level $\zeta$ and a distance of $\Delta z$ below the peak water level. Storm data were selected from time series with measured water levels, and a mean value and standard deviation of the load duration were determined for different values of $\Delta z$. The wave impact zone is assumed to range between still water level and 0.5 times the significant wave height below still water level. Outside this range, there is no wave impact (De Waal and Van Hoven, 2015). Application of a uniform distribution of the water level over $\Delta z$ leads to the following expression for the effective load duration (hrs):

$$t_{load,eff} = t_{load}\min\left(\frac{H_{m0}}{2\Delta z}; 1\right). \tag{14}$$

Test simulations showed that the failure probability gradually decreases with increasing $\Delta z$, as long as $\Delta z > H_{m0}/2$. The dependence is only weak. Even extremely strong grass covers cannot withstand waves higher than 2.0 m. Therefore, a value of $\Delta z = 2.0/2 = 1.0$ m is selected. The location on the dike slope with the highest probability of exceedance of $Z < 0$ can not be determined beforehand, but follows from the probabilistic computations.

## Appendix C. Failure due to wave impact on asphalt revetments

This appendix summarizes the formulas describing dike failure due to wave impact on asphalt revetments. Equations are based on De Waal and Van Hoven (2015). The bending stress $\sigma$ in Eq. (5) depends on the characteristics of the wave impact, the distance along the slope from the considered position on the asphalt layer to the location with the maximum wave impact, the asphalt characteristics, and the characteristics of the subsoil. According to De Looff et al. (2006), the asphalt layer is schematized as an elastic supported beam with small springs, loaded by a triangular-shaped wave impact. The asphalt layer (schematized as beam) is characterized by a thickness $d_a$ (m), a flexural strength $\sigma_{br}$ (MPa) and a stiffness modulus $S_a$ (N/m$^2$). Elastic support is provided by the subsoil, which is usually sand. The elasticity of the subsoil is described by a modulus of subsoil reaction $c_{sub}$ (N/m$^3$). These characteristics are combined into a parameter $\beta$, which reads

$$\beta = \sqrt[4]{\frac{3c_{sub}(1 - \nu^2)}{S_a d_a^3}}, \tag{15}$$

where $\nu$ (−) is the Poisson's ratio of asphalt.The maximum wave impact can be calculated with a formula, originally proposed by Führböter and Sparboom (1988):

$$p_{max} = 4\tan(\alpha_d)\rho g q_p H_{m0}, \tag{16}$$

where $q_p$ is an impact factor (−) to account for the variability in wave impact of individual waves, given a significant wave height $H_{m0}$, $\rho$ is the mass density of water (kg/m$^3$), and $g$ is the gravitational acceleration (m/s$^2$). The impact factor $q_p$ is described by a log-normal distribution with mean value 3.1 and standard deviation 0.72. Besides of the impact factor, individual waves also vary in position of the maximum impact with respect to still water level, and in the width of the triangular-shaped wave load. The position of the maximum wave impact equals $D_p = d_p H_{m0}$, in which the factor $d_p$ follows a normal distribution with mean value −0.50 and standard deviation 0.25. This implies that the position of the maximum wave impact is on average half of the significant wave height below still water level. Also the width of the wave load scales with the wave height, via $B_p = b_p H_{m0}$, where $b_p$ is log-normally distributed, with mean value 0.65 and standard deviation 0.45. These distributions are continuous representations of the discrete probability distributions, given in De Looff et al. (2006).Analogue to the model for grass covers, a layer height $\Delta z$ is considered, with a corresponding load duration $t_{load}$ (hrs). The number of waves $N_w$ in Eq. (7) is equal to $3600t_{load}/T_{mean}$, where $T_{mean}$ is the mean wave period (s). A random water level between $\zeta$ and $\zeta$-$\Delta z$ is assigned to all $N_w$ waves, and combined with a realization from the probability distributions of $q_p$, $d_p$ and $b_p$. The same random realizations are used in all computations, to increase stability in the probabilistic computations. The most impacted point is situated at $z = \zeta - 0.5H_{m0}$, according to the distribution of $d_p$. The layer height $\Delta z$ should be large enough, to guarantee that waves at water levels outside the layer do not generate significant bending stresses at $z = \zeta - 0.5H_{m0}$. However, for a very large layer height $\Delta z$, a long storm duration is found, although with only a small fraction of the waves causing high stresses at $z = \zeta - 0.5H_{m0}$. Test simulations showed that results are nearly identical for approximately $\Delta z > 0.7$ m, so $\Delta z$ is set to 1.0 m. All $N_w$ waves cause a bending stress $\sigma$ at this point, which depends on the distance along the slope $x$ ($x \geq 0$) between this point to the position of the maximum wave impact (the center of the triangular-shaped load) via the equations given in De Looff et al. (2006), which depend on $p_{max}$, $\beta$, $B_p$, $x$ and $d_a$.

# References

Adam, P., 2002. Saltmarshes in a time of change. Environ. Conserv. 29 (1), 39–61.

Allen, J.R.L., 2000. Morphodynamics of holocene salt marshes: a review sketch from the atlantic and southern North sea coasts of Europe. Quat. Sci. Rev. 19 (12), 1155–1231.

Arns, A., Dangendorf, S., Jensen, J., Talke, S., Bender, J., Pattiaratchi, C., 2017. Sea-level rise induced amplification of coastal protection design heights. Sci. Rep. 7, 40171.

Bakker, J.P., Esselink, P., Dijkema, K.S., Van Duin, W.E., De Jong, D.J., 2002. Restoration of salt marshes in The Netherlands. Hydrobiologia 478, 29–51.

Battjes, J.A., Janssen, J.P.F.M., 1978. Energy loss and set-up due to breaking of random waves. In: Proceedings of 16th International Conference on Coastal Engineering, Am. Soc. Of Civ. Eng, pp. 569–587. New York, 32(1).

Battjes, J.A., Stive, M.J.F., 1985. Calibration and verification of a dissipation model for random breaking waves. J. Geophys. Res. 90 (C5), 649–660.

Booij, N., Ris, R.C.R., Holthuijsen, L.H.L., 1999. A third-generation wave model for coastal regions. I- Model description and validation. J. Geophys. Res. 104 (C4), 7649.

Borsje, B.W., Vries, S.D., Janssen, S.K.H., Luijendijk, A.P., Vuik, V., de Vries, S., Janssen, S.K.H., Luijendijk, A.P., Vuik, V., 2017. Building with Nature as Coastal Protection Strategy in the Netherlands. Living Shorelines: the Science and Management of Nature-based Coastal Protection, 1 edition. CRC Press, pp. 137–155.

Bouma, T.J., van Belzen, J., Balke, T., Zhu, Z., Airoldi, L., Blight, A.J., Davies, A.J., Galvan, C., Hawkins, S.J., Hoggart, S.P.G., Lara, J.L., Losada, I.J., Maza, M., Ondiviela, B., Skov, M.W., Strain, E.M., Thompson, R.C., Yang, S., Zanuttigh, B., Zhang, L., Herman, P.M.J., 2014. Identifying knowledge gaps hampering application of intertidal habitats in coastal protection: opportunities & steps to take. Coast. Eng. 87, 147–157.

Bradshaw, C.J.A., Sodhi, N.S., Peh, K.S.H., Brook, B.W., 2007. Global evidence that deforestation amplifies flood risk and severity in the developing world. Global Change Biol. 13 (11), 2379–2395.

Bretschneider, C.L., Krock, H.J., Nakazaki, E., Casciano, F.M., 1986. Roughness of Typical Hawaiian Terrain for Tsunami Run-up Calculations: a Users Manual. Report No. University of Hawaii, Honolulu.

Bridges, T.S., Wagner, P.W., Burks-copes, K.A., Bates, M.E., Collier, Z.A., Fischenich, C.J., Gailani, J.Z., Leuck, L.D., Piercy, C.D., Rosati, J.D., Russo, E.J., Shafer, D.J., Suedel, B.C., Vuxton, E.A., Wamsley, T.V., 2015. Use of Natural and Nature-based Features (NNBF) for Coastal Resilience. Report No. ERDC SR-15–1. US Army Corps of Engineers - Engineer Research and Development Center.

Buijs, F.A., Van Gelder, H.A.J.M., Hall, J.W., 2004. Application of reliability-based flood defence design in the UK. Heron 49 (1), 33–50.

Carsell, K.M., Pingel, N.D., Ford, D.T., 2004. Quantifying the benefit of a flood warning system. Nat. Hazards Rev. 5 (3), 131–140.

Chbab, H., Groeneweg, J., 2015. Modelonzekerheid Belastingen [Model Uncertainty Hydraulic Loads]. Report No. 1209433-008. Deltares, Delft, The Netherlands.

De Looff, A.K., t Hart, R., Montauban, K., Van de Ven, M.F., 2006. Golfklap, a model to determine the impact of waves on dike structures with an asphalt concrete layer. In: Coastal Engineering Proceedings, vol. 30, pp. 1–10. San Diego.

De Waal, J.P., Van Hoven, A., 2015. Failure Mechanism Module Grass Wave Impact Zone; Requirements and Functional Design. Report No. 1220043-002. Deltares, Delft, The Netherlands.

Deegan, L.A., Johnson, D.S., Warren, R.S., Peterson, B.J., Fleeger, J.W., Fagherazzi, S., Wollheim, W.M., 2012. Coastal eutrophication as a driver of salt marsh loss. Nature 490 (7420), 388–392.

Den Heijer, C.K., Baart, F., van Koningsveld, M., Den Heijer, K., Baart, F., van Koningsveld, M., Den Heijer, C.K., Baart, F., van Koningsveld, M., 2012. Assessment of dune failure along the Dutch coast using a fully probabilistic approach. Geomorphology 143–144, 95–103.

Duarte, C.M., Losada, I.J., Hendriks, I.E., Mazarrasa, I., Marba, N., 2013. The role of coastal plant communities for climate change mitigation and adaptation. Nat. Clim. Change 3 (11), 961–968.

EurOtop, 2016. EurOtop 2016: Manual on Wave Overtopping of Sea Defences and Related Structures an Overtopping Manual Largely Based on European Research, but for Worldwide Application. Van der Meer, J.W.; Allsop, N.W.H.; Bruce, T.; De Rouck, J.; Kortenhaus, A.; Pullen, T.; Schüttrumpf, H.; Troch, P.; Zanuttigh, B.

Francalanci, S., Bendoni, M., Rinaldi, M., Solari, L., 2013. Ecomorphodynamic evolution of salt marshes: experimental observations of bank retreat processes. Geomorphology 195, 53–65.

Führböter, A., Sparboom, U., 1988. Shock pressure interactions on prototype sea dykes caused by breaking waves. In: Proc. SOWAS '88 (Modelling Soil-water-structure Interactions). ISBN 90.6191.8154.

Gedan, K.B., Kirwan, M.L., Wolanski, E., Barbier, E.B., Silliman, B.R., 2011. The present and future role of coastal wetland vegetation in protecting shorelines: answering recent challenges to the paradigm. Climatic Change 106 (1), 7–29.

Groeneweg, J., Beckers, J., Gautier, C., 2010. A probabilistic model for the determination of hydraulic boundary conditions in a dynamic coastal system. In: Coastal Engineering Proceedings, vol. 32. China, Shanghai, pp. 1–13.

Hall, J.W., Meadowcroft, I.C., Lee, E.M., Van Gelder, P.H.A.J.M., 2002. Stochastic simulation of episodic soft coastal cliff recession. Coast. Eng. 46 (3), 159–174.

Hasofer, A.M., Lind, N.C., 1974. Exact and invariant second-moment code format. J. Eng. Mech. Div. 100 (1), 111–121.

Hofland, B., Chen, X., Altomare, C., Oosterlo, P., 2017. Prediction formula for the spectral wave period Tm-1,0 on mildly sloping shallow foreshores. Coast. Eng. 123, 21–28.

Hu, Z., Suzuki, T., Zitman, T.J., Uittewaal, W., Stive, M.J.F., Uijttewaal, W.S.J., Stive, M.J.F., 2014. Laboratory study on wave dissipation by vegetation in combined current-wave flow. Coast. Eng. 88, 131–142.

Jones, H.P., Hole, D.G., Zavaleta, E.S., 2012. Harnessing nature to help people adapt to climate change. Nat. Clim. Change 2 (7), 504–509.

Jongejan, R.B., Stefess, H., Roode, N., Horst, W., Maaskant, B., 2011. The VNK2 project: a detailed, large-scale quantitative flood risk analysis for The Netherlands. In: International Conference on Flood Management, vol. 5, pp. 27–29.

Jonkman, S.N., Kok, M., Vrijling, J.K., 2008. Flood risk assessment in The Netherlands: a case study for dike ring South Holland. Risk Anal. 28 (5), 1357–1373.

Kanning, W., Den Hengst, S., 2013. Probabilistic Assessment of Asphalt Revetments in the WTI2017. Report No. 1207805-007. Deltares, Delft, The Netherlands.

Kirwan, M.L., Megonigal, J.P., 2013. Tidal wetland stability in the face of human impacts and sea-level rise. Nature 504 (7478), 53–60.

Klerk, W.J., Jongejan, R.B., 2016. Semi-probabilistic Assessment of Wave Impact and Runup on Grass Revetments. Report No. 1220080-005. Deltares, Delft, The Netherlands.

Kolen, B., Helsloot, I., 2014. Decision-making and evacuation planning for flood risk management in The Netherlands. Disasters 38 (3), 610–635.

Komen, G.J., Hasselmann, K., Hasselmann, K., 1984. On the existence of a fully developed wind-sea spectrum. J. Phys. Oceanogr. 14 (8), 1271–1285.

Kruse, G.A.M., 2010. Studie Voor Richtlijnen Klei Op Dijktaluds in Het Rivierengebied [Study for Guidelines for Clay on Dike Slopes in Riverine Areas]. Report No. 1202512-000. Deltares, Delft, The Netherlands.

Lo, V.B., Bouma, T.J., van Belzen, J., Van Colen, C., Airoldi, L., 2017. Interactive effects of vegetation and sediment properties on erosion of salt marshes in the Northern Adriatic Sea. Mar. Environ. Res. 131, 32–42.

Lopez, J., 2009. Contribution on the holocene reconstruction of the multiple lines of defense strategy to sustain coastal Louisiana the multiple lines of defense strategy to sustain coastal Louisiana. J. Coast Res. 54, 186–198.

Luhar, M., Nepf, H.M., 2011. Flow-induced reconfiguration of buoyant and flexible aquatic vegetation. Limnol. Oceanogr. 56 (6), 2003–2017.

Madsen, O.S., Poon, Y.-K., Graber, H.C., 1988. Spectral wave attenuation by bottom friction: theory. In: Proceedings of the 21th Int. Conf. Coastal Engineering, pp. 492–504.

Mckee, K.L., Cahoon, D.R., Feller, I.C., 2007. Caribbean mangroves adjust to rising sea level through biotic controls on change in soil elevation. Global Ecol. Biogeogr. 16 (5), 545–556.

Mendelsohn, R., Emanuel, K., Chonabayashi, S., Bakkensen, L., 2011. The impact of climate change on global tropical storm damages. Nat. Clim. Change 2 (February), 1–39.

Mendez, F.J., Losada, I.J., 2004. An empirical model to estimate the propagation of random breaking and nonbreaking waves over vegetation fields. Coast. Eng. 51 (2), 103–118.

Merz, B., Thieken, A.H., 2005. Separating natural and epistemic uncertainty in flood frequency analysis. J. Hydrol. 309 (1–4), 114–132.

Möller, I., Kudella, M., Rupprecht, F., Spencer, T., Paul, M., van Wesenbeeck, B.K., Wolters, G., Jensen, K., Bouma, T.J., Miranda-Lange, M., Schimmels, S., 2014. Wave attenuation over coastal salt marshes under storm surge conditions. Nat. Geosci. 7 (10), 727–731.

Mudd, S.M., D'Alpaos, A., Morris, J.T., 2010. How does vegetation affect sedimentation on tidal marshes? Investigating particle capture and hydrodynamic controls on biologically mediated sedimentation. J. Geophys. Res.: Earth Surf. 115 (3), 1–14.

Reise, K., Baptist, M., Burbridge, P., Dankers, N., Fischer, L., Flemming, B., Oost, A.P., Smit, C., 2010. The Wadden Sea Quality Status Report- Synthesis Report. Report No. 29. Common Wadden Sea Secretariat, Wilhelmshaven, Germany.

Rosenblatt, M., 1952. Remarks on a multivariate transformation. Ann. Math. Stat. 23 (3), 470–472.

Rupprecht, F., Möller, I., Paul, M., Kudella, M., Spencer, T., van Wesenbeeck, B.K., Wolters, G., Jensen, K., Bouma, T.J., Miranda-Lange, M., Schimmels, S., 2017. Vegetation-wave interactions in salt marshes under storm surge conditions. Ecol. Eng. 100, 301–315.

Salvadori, G., Durante, F., Tomasicchio, G.R., D'Alessandro, F., 2015. Practical guidelines for the multivariate assessment of the structural risk in coastal and off-shore engineering. Coast. Eng. 95, 77–83.

Salvadori, G., Tomasicchio, G.R., D'Alessandro, F., 2014. Practical guidelines for multivariate analysis and design in coastal and off-shore engineering. Coast. Eng. 88, 1–14.

Scussolini, P., Aerts, J.C.J.H., Jongman, B., Bouwer, L.M., Winsemius, H.C., De Moel, H., Ward, P.J., 2016. FLOPROS: an evolving global database of flood protection standards. Nat. Hazards Earth Syst. Sci. 16 (5), 1049–1061.

Sebastian, A., Dupuits, E.J., Morales-Nápoles, O., 2017. Applying a Bayesian network based on Gaussian copulas to model the hydraulic boundary conditions for hurricane flood risk analysis in a coastal watershed. Coast. Eng. 125 (January), 42–50.

Snyder, R.L., Dobson, F.W., Elliott, J.A., Long, R.B., 1981. Array measurements of atmospheric pressure fluctuations above surface gravity waves. J. Fluid Mech. 102, 1–59.

Spalding, M.D., Mcivor, A.L., Beck, M.W., Koch, E.W., Möller, I., Reed, D.J., Rubinoff, P., Spencer, T., Tolhurst, T.J., Wamsley, T.V., van Wesenbeeck, B.K., Wolanski, E., Woodroffe, C.D., 2014. Coastal ecosystems: a critical element of risk reduction. Conserv. Lett. 7 (3), 293–301.

Spencer, T., Brooks, S.M., Evans, B.R., Tempest, J.A., Möller, I., 2015. Southern North Sea storm surge event of 5 December 2013: water levels, waves and coastal impacts. Earth Sci. Rev. 146, 120–145.

Spencer, T., Möller, I., Rupprecht, F., Bouma, T.J., van Wesenbeeck, B.K., Kudella, M., Paul, M., Jensen, K., Wolters, G., Miranda-Lange, M., Schimmels, S., 2016. Salt marsh surface survives true-to-scale simulated storm surges. Earth Surf. Process. Landforms 41 (4), 543–552.

Steenbergen, H.M.G.M., Lassing, B.L., Vrouwenvelder, A.C.W.M., Waarts, P.H., 2004. Reliability analysis of flood defence systems. Heron 49 (1), 51–73.

Van der Meer, J.W., Schrijver, R., Hardeman, B., Hoven, A.V., Verheij, H., Steendam, G.J., 2009. Guidance on erosion resistance of inner slopes of dikes from three years of testing with the Wave Overtopping Simulator. In: Proc. ICE 2009, vol. 162, pp. 1–14.

Van Gelder, P., 2000. Statistical Methods for the Risk-based Design of Civil Structures. Phd thesis. Delft University of Technology, Delft, The Netherlands.

Van Koningsveld, M., De Boer, G.J., Baart, F., Damsma, T., Den Heijer, C., Van Geer, P., De Sonnevile, B., 2010. OpenEarth: Inter-company Management of: Data, Models, Tools and Knowledge. WODCON XIX: Dredging Makes the World a Better Place, 14 pp.

van Loon-Steensma, J.M., 2015. Salt marshes to adapt the flood defences along the Dutch Wadden Sea coast. Mitig. Adapt. Strategies Glob. Change 20 (6), 929–948.

van Wesenbeeck, B.K., de Boer, W., Narayan, S., van der Star, W.R., de Vries, M.B., 2017. Coastal and riverine ecosystems as adaptive flood defenses under a changing climate. Mitig. Adapt. Strategies Glob. Change 22 (7), 1087–1094.

Van Wesenbeeck, B.K., Mulder, J.P.M., Marchand, M., Reed, D.J., de Vries, M.B., De Vriend, H.J., Herman, P.M.J., 2014. Damming deltas: a practice of the past? Towards nature-based flood defenses. Estuar. Coast Shelf Sci. 140, 1–6.

Voortman, H.G., 2003. Risk-based Design of Large-scale Flood Defence Systems. Phd thesis. Delft University of Technology, Delft, The Netherlands.

Vrijling, J.K., 2001. Probabilistic design of water defense systems in The Netherlands. Reliab. Eng. Syst. Saf. 74 (3), 337–344.

Vuik, V., Jonkman, S.N., Borsje, B.W., Suzuki, T., 2016. Nature-based flood protection: the efficiency of vegetated foreshores for reducing wave loads on coastal dikes. Coast. Eng. 116, 42–56.

Vuik, V., Suh Heo, H.Y., Zhu, Z., Borsje, B.W., Jonkman, S.N., 2018. Stem breakage of salt marsh vegetation under wave forcing: a field and model study. Estuar. Coast Shelf Sci. 200, 41–58.

Vuik, V., van Balen, W., van Vuren, S., 2017. Fully probabilistic assessment of safety against flooding along the Dutch coast. J. Flood Risk Manag. 10 (3), 349–360.

Walker, W., Harremoës, P., Rotmans, J., Van der Sluijs, J., Van Asselt, M., Janssen, P., Krayer von Krauss, M., 2003. Defining uncertainty: a conceptual basis for uncertainty management in model-based decision support. Integrated Assess. 4 (1), 5–17.

Wamsley, T.V., Cialone, M.A., Smith, J.M., Atkinson, J.H., Rosati, J.D., 2010. The potential of wetlands in reducing storm surge. Ocean Eng. 37 (1), 59–68.

Willemsen, P.W., Horstman, E.M., Borsje, B.W., Friess, D.A., Dohmen-Janssen, C.M., 2016. Sensitivity of the sediment trapping capacity of an estuarine mangrove forest. Geomorphology 273, 189–201.

Zhang, L., Xu, Y., 2011. Assessment of levee breaching risks to the pearl river delta. In: Vogt, N., Schuppener, B., Straub, D., Bräu, G. (Eds.), Geotechnical Safety and Risk. ISGSR 2011, pp. 613–621. Karlsruhe, BAW.

Zhao, B., Kreuter, U., Li, B., Ma, Z., Chen, J., Nakagoshi, N., 2004. An ecosystem service value assessment of land-use change on Chongming Island, China. Land Use Pol. 21 (2), 139–148.